https://doi.org/10.5194/egusphere-2025-1228
Preprint. Discussion started: 28 March 2025

Archaeal lipostratigraphy of the Scotian Slope shallow sediments, Atlantic Canada

Narges Ahangarian[1], Unyime Umoh[1], Natasha MacAdam[2], Adam MacDonald[2], Patricia Granados[3], Jeremy N. Bentley[1], Elish Redshaw[1], Martin G. Fowler[4], Venus Baghalabadi[1,5], G. Todd Ventura[1]

[1]Department of Geology, Saint Mary's University, 923 Robie Street, Halifax, Nova Scotia B3H 3C3, Canada
[2]Nova Scotia Department of Energy, 1690 Hollis St., Halifax, Nova Scotia B3J 3J9, Canada
[3]Centre for Environmental Analysis and Remediation, Saint Mary's University, 923 Robie Street, Halifax, Nova Scotia B3H 3C3, Canada
[4]Applied Petroleum Technology (Canada) Ltd., Calgary, AB T3A 2M3, Canada
[5]Department of Pharmacology, Dalhousie University, 5850 College St, Halifax, Nova Scotia, B3H 4R2, Canada

Correspondence to: Narges Ahangarian (Narges.ah@hotmail.com), G. Todd Ventura (todd.ventura@smu.ca)

Abstract. The Scotian Slope in the North Atlantic Ocean extends ~500 km along the coast of Nova Scotia, Canada, descending from 400 m to 5 km water depth. With a maximum sediment thickness of ~24 km, large portions of the deeper basin are affected by salt tectonism, which has greatly impacted the basin stratigraphy and locally facilitated hydrocarbon seepage to the ocean seafloor. The surface sediments along the slope may therefore be home to microbial communities, which respond to complex geochemical drivers that not only include communication with the overlying water column, but also potential advection of deeper basinal fluids. Archaea are fundamental components of these communities, and their lipids act as important indicators of environmental conditions and microbial interactions within marine sediments. This study evaluates the spatial abundance and diversity of archaeal lipids preserved in shallow buried Scotian Slope sediments to better understand deep marine archaea community dynamics. Seventy-four sediment samples from 32 gravity and piston cores reaching a maximum depth of 9 meters below seafloor (mbsf) were collected during three survey cruises across a large region of the Scotian Slope. The survey area extends across ~40,000 km^2, marking ~3° of latitudinal change over a water column depth that increases from ~1500 to 3500 m, of which one sampling site was a suspected cold seep environment. In total, 14 archaeal lipid classes comprising 42 unique compounds were detected. The lipid distributions reflect a high contribution of anaerobic methanotrophic (ANME) archaeal groups, such as ANME-1 to -3. Hierarchical cluster analysis (HCA) and principal components analysis (PCA) were used to show varying contributions of four lipid classes that included distinct assemblages of intact polar lipids (IPLs), which are largely sourced from living cells as well as core lipids (CLs), and their degradation products (CL-DPs) that collectively are sourced from different alteration stages following the death of the cell. From this, four stratigraphically distinct archaeal lipidomes, marking varying relative abundances of the lipid classes were observed in the upper 9 m of the surveyed slope sediments. One lipidome likely reflects archaeal communities impacted by a cold seep based on hydrocarbon head space gas analyses and high methane index and GDGT/Cren ratios. The other three lipidomes occur across overlapping sediment depth intervals in which the diversity and abundance of living, fossil, and degraded core lipids systematically change in what is likely depth. These changes likely mark systematic geochemically controlled, microbial

https://doi.org/10.5194/egusphere-2025-1228
Preprint. Discussion started: 28 March 2025

community variations that are accompanying an increasing stockpile of diagenetic altered CLs. The three ambient sediment lipidomes appear to be highly conserved across the latitudinal extent of the study area marking a resolvable shallow sediment lipostratigraphy for the Scotian Slope.

1 Introduction

The Scotian Slope marks a portion of the North American continental shelf that extends for ~500 km along the eastern coastal seaboard of Nova Scotia (Fig. 1). The slope descends from ~400 m at the shelf edge to water depth near the abyssal plain. The depositional history of the basin began in the Late Triassic leading to 250 million years of continuous sedimentation with the maximum sediment thickness reaching 24 km (Wade and MacLean 1990). Deep basin salt tectonic movement within the Scotian Margin has caused localized changes to the sub-basin stratigraphy resulting in the breaking of petroleum reservoir seals (i.e., Deptuck and Kendall, 2017; 2020) leading to the prediction of hydrocarbons seeps on the ocean floor. Multiple geophysical and geochemical surveys have identified potential seep sites on the ocean floor (Campbell, 2019; Fowler, 2017). Yet, it is not clear to what extent microbial communities are impacted by seepage in shallow ocean bottom sediments.

In this regard, the Scotian Slope is an ideal region for examining the interplay between organic matter preservation and microbial interactions, both of which are critical in global carbon cycling. Genomic analyses, including 16S rRNA amplicon sequencing and metagenomic profiling, have been used to resolve the diverse microbial communities inhabiting surface and shallow buried sediments within the deep marine sediments of this area. Bacteria including Proteobacteria, Desulfobacterota, and Caldatribacteriota are the most abundant phyla across various sediment strata (Zorz et al., 2023) with prominent lineages such as Gammaproteobacteria, Deltaproteobacteria, and Alphaproteobacteria detected in shallow sediments and deeper buried sediments being dominated by Atribacteria, Chloroflexi, and Deltaproteobacteria (Dong et al., 2020). Of the archaeal domain, members of Thaumarchaeota dominate the shallow and surface sediments and their abundance decreases in deeper strata, while phyla such as Methanomicrobia and Lokiarchaeota mark the dominate taxa in deeper buried sediments (Dong et al., 2020). Archaeal communities such as ANME-1 and ANME-2, which play important roles in the anaerobic oxidation of methane, are prominent at depths corresponding to the sulfate-methane transition zone (Dong et al., 2020). The metabolic specificity of these organisms alongside their community composition can be strong indicators to the presence of hydrocarbon seepage at targeted Scotian Slope sites (Dong et al., 2020; Gittings et al., 2022; Li et al., 2023). For example, in the shallow sediments at hydrocarbon seep sites, microbial communities capable of oxidizing C2+ alkanes dominate (Zorz et al., 2023). Additionally, microbial communities in sediments close to cold seeps can be enriched in thermophilic bacterial endospores, which indicates a mixing of deeper biosphere into the shallow marine sediment realm (Gittings et al., 2022; Rattray et al., 2023). As such, the complex microbial communities inhabiting these sediments are characterized as being depth stratified and further influenced by hydrocarbon seepage (Li et al., 2023).

Deep marine sediments are globally extensive, complex, and dynamic biogeochemical interfaces, which serve as sinks for carbon and nutrients (Burdige, 2007). The interaction between microbial communities and sedimentary processes within these

https://doi.org/10.5194/egusphere-2025-1228
Preprint. Discussion started: 28 March 2025

environments is a key component of nutrient cycling, organic matter degradation, and environmental changes over geological timescales (Orcutt et al., 2011). A major microbial driver of these processes are archaea, which are ubiquitous in deep marine sediments (Sturt et al., 2004; Fredricks and Hinrichs, 2007; Lipp et al., 2008; Hoshino et al., 2020; Lipp and Hinrichs, 2009; Biddle et al., 2006). Archaea play critical roles in the transformation of carbon and nitrogen (Offre et al., 2013). Their ability to adapt to diverse and extreme conditions makes them important subjects in the study of life's extremes and global ecological processes (Valentine, 2007; Sollich et al., 2017).

The unique membrane lipid structures of archaea differ from bacteria and eukarya (e.g., Koga et al., 1993; De Rosa, 1996). Archaeal membrane lipids are formed from isoprenoidal hydrocarbon chain to the glycerol backbone through ether bonds (De Rosa, 1996). IPLs are phospholipids and glycolipids with polar headgroups that indicate active, or recently active, microbial cells (Sturt et al., 2004; Schouten et al., 2010). In contrast, CLs are degraded remnants of IPLs and are informative in past microbial communities (White et al., 1979). IPLs are generally considered to reflect the present-day microbial community, while CLs can be remnants of past communities or altered products of IPLs over time (White et al., 1979; Lipp and Hinrichs, 2009; Schouten et al., 2013). Therefore, variation between CL and IPL ratios can indicate shifts in microbial community structure and function with sediment depth by diagenesis (Biddle et al., 2006; Schouten et al., 2013). The composition and distribution of lipid biomarkers, particularly IPLs and CLs, are important in studying marine sediments for tracing microbial life and environmental conditions (Koelmel et al., 2020). Archaeal lipids, a subset of these biomarkers, are significant in marine sediments (Sturt et al., 2004; Biddle et al., 2006). The unique compounds like glycerol dialkyl glycerol tetraethers (GDGTs) can serve as indicators of archaeal activity and in reconstructing past environmental conditions (Schouten et al., 2002; Kim et al., 2010).

For this study, the diversity and abundance of archaeal lipids extracted from shallow ocean floor sediments of the Scotian Slope are examined to provide further insights into the microbial processes of deep marine sedimentary systems. The resolvable lipidomes are examined across three spatial dimensions: sediment depth, distance down the continental slope, and along ~3° latitude change of the northwestern trend of the continental margin. The resolved lipidomes are then compared with several sedimentological, geochemical, archaeal lipid proxy ratios to better constrain the microbial community structure and function within the sediments.

2 Materials and methods

2.1 Sample collection

Seventy-four sediment samples were selected from 32 piston and gravity cores collected during three survey cruises that took place in 2015, 2016, and 2018 aboard the CCGS Hudson research vessel (Fig. 1 and Table 1). Of these, 17 sediment samples were acquired from 12 piston cores during the 2015 expedition. Twenty-four sediment samples were taken from 16 piston cores during the 2016 cruise and 33 sediment samples were obtained from four gravity cores during the 2018 cruise. A 10 m piston corer was used for the 2015 and 2016 cruises (Campbell and MacDonald 2016; Campbell 2019). The 2018 cruise used

https://doi.org/10.5194/egusphere-2025-1228
Preprint. Discussion started: 28 March 2025

a gravity corer that extended 6 m in length. Cores were immediately sectioned into 1.5 m long intervals on-board the ship and inspected for diagnostic signs of hydrocarbon seepage (e.g., gas cracks, bubbling, or strong odours; Campbell and Normandeau 2019). Sediment within 20 cm of the base of each core was scooped into a 500 mL IsoJar (Isotech Laboratories, Inc.), flushed with nitrogen, sealed, and stored at -20˚C for hydrocarbon biomarker and headspace gas analyses (Fowler et al., 2017). The remaining full-length cores were then split longitudinally with a core splitter and further inspected for lithology, obvious hydrocarbon staining, and evidence of gas. Samples for geochemical analyses were wrapped in aluminium foil, sealed in Whirl-pack® bags, and frozen at -80˚C on board the ship. These samples were kept frozen until analysed at the land-based laboratories. Information regarding the specific sampling sites is available in cruise reports (Campbell and MacDonald 2016; Campbell 2019; and Campbell and Normandeau 2019). Among these samples, core "2018, 0007" (Table 2) collected from a gravity core that targeted a suspected cold seep site (Campbell and Normandeau 2019) appears to have been impacted by hydrocarbon seepage based on additional geochemical evidence (Fowler et al., 2018). Several other cores had sediment intervals that potentially indicated the presence of hydrocarbons (Table 1) that were far away from the sampled intervals investigated in this study. Lithologic information was extracted from the open file cruise report Jenner et al. (2022) for core samples collected on 2015 expedition cruise. Sediment lithologic information for the other samples were provided by GSC Atlantic, NRCAN for cores collected during the 2016 and 2018 expedition cruises and are recorded in supplemental Table S1.

2.2 Bulk sediment geochemistry

Approximately 10 g of the frozen sediment was weighed, desiccated in a drying oven at 30˚C, and reweighted to obtain its dry weight. The dried sediment was powdered using a mortar and pestle and acid digested in 6N H_3PO_4 solution for 4 days. Once the inorganic carbon was removed, the sediment was flushed with Milli-Q water, transformed into a slurry using a vortex mixer, and centrifugated at 1250 rpm for 7 min. The supernatant was decanted. This process was repeated until the sediment was renormalized. Decarbonated sediments were then subsampled for bulk geochemical analysis to constrain organic matter source and diagenetic changes with sediment depth (Fig. 2). Sediment total organic carbon (TOC) and total nitrogen (TN) was measured using a Perkin-Elmer 2400 Series II CHNS/O Elemental Analyzer (EA) located in the Centre for Environmental Assessment and Remediation at Saint Mary's University. Stable carbon isotope of TOC ($\delta^{13}C_{TOC}$) measurements was made at the University of Calgary.

Table 1: Scotian Slope samples.

Sample name	Sample ID[a]	Sample type[b]	Core type	Lat.	Long.	Water depth (m)	Top core sample depth (cmbsf)	Bottom core sample depth (cmbsf)	$TOC_{predicted}$ (wt. %)	$TOC_{adjusted}$ (wt. %)	TN (wt. %)	$\delta^{13}C_{TOC}$ (‰)	Extracted sediment (g)	TLE (μg g^{-1} $sed.^{-1}$)	Hydrocarbon detection[c]
2015-1, 180	NSPC-2015018-001-S01B	Mud	Piston	42.112938	-64.405270	2082	172	178	0.7	1.1	0.09	-	20.1	546	Ambient
2015-3, 490	NSPC-2015018-003-S03B	Mud	Piston	42.052693	-64.700207	2016	485	491	0.4	1.0	0.06	-	20.22	255	Ambient
2015-4, 600	NSPC-2015018-004-S04 B	Mud	Piston	42.310843	-63.886528	1763	594	599	-	-	-	-	20.31	176	Ambient
2015-6, 220	NSPC 2015018-0006 S01 B	Mud	Piston	41.927130	-63.716420	2648	220	226	0.7	1.3	0.07	-	20.14	251	Ambient
2015-6, 330	NSPC 2015018-0006 S02 B	Mud	Piston	41.927130	-63.716420	2648	328	333	0.7	1.3	0.07	-	20.29	375	
2015-6, 360	NSPC 2015018-0006 S03 B	Mud	Piston	41.927130	-63.716420	2648	360	365	0.4	0.9	0.04	-	20.4	302	

https://doi.org/10.5194/egusphere-2025-1228
Preprint. Discussion started: 28 March 2025

2015-6, 500	NSPC 2015018-0006 S04 B	Mud	Piston	41.927130	-63.716420	2648	500	505	0.5	1.1	0.07	-	20.19	822	
2015-8, 750	NSPC-2015018-008-S03 B	Mud	Piston	42.097695	-63.693832	2360	739	744	0.1	0.8	0.06	-	20.74	358	Ambient
2016-1, 630	2016011-001 S03 B	Mud	Piston	41.724833	-64.796127	2533	631	636	0.3	0.9	0.03	-	20	185	Ambient
2016-3, 160	2016011-003 S01 B	Mud	Piston	41.804088	-64.869017	2376	160	165	0.4	0.8	0.09	-	20.18	144	Ambient
2016-12, 640	2016011-012 S03 B	Mud	Piston	42.293287	-63.997142	1760	640	645	0.4	1.1	0.09	-	20.08	222	Ambient
2016-14, 300	2016011-014 S01 B	Mud	Piston	41.927357	-63.716940	2585	295	300	0.3	0.9	0.06	-	20.13	298	Ambient
2016-14, 380	2016011-014 S02 B	Mud	Piston	41.927357	-63.716940	2585	375	380	0.5	1.0	0.04	-	20.06	170	
2016-14, 400	2016011-014 S03 B	Mud	Piston	41.927357	-63.716940	2585	399	404	0.3	0.9	0.05	-	20.02	94	
2016-14, 580	2016011-014 S04 B	Mud	Piston	41.927357	-63.716940	2585	573	578	-	-	-	-	20.09	114	
2016-14, 780	2016011-014 S05 B	Mud	Piston	41.927357	-63.716940	2585	775	780	0.3	0.9	0.07	-	20.12	107	
2016-14, 870	2016011-014 S06 B	Mud	Piston	41.927357	-63.716940	2585	871	876	0.2	0.8	0.05	-	20.05	100	
2015-9, 150	NSPC 2015018-0009 S01 B	Mud	Piston	42.308610	-62.836325	2284	144	149	0.5	0.9	0.05	-	20.73	123	Ambient
2015-9, 300	NSPC 2015018-0009 S03 B	Mud	Piston	42.308610	-62.836325	2284	297	302	0.4	0.9	0.06	-	20.95	437	
2015-9, 370	NSPC 2015018-0009 S04 B	Mud	Piston	42.308610	-62.836325	2284	363	369	0.4	1.0	0.02	-	20.52	500	
2015-11, 350	NSPC-2015018-011-S03 B	Mud	Piston	42.270058	-62.938060	2327	346	351	0.4	0.9	0.05	-	20.57	245	Ambient
2015-12, 700	NSPC-2015018-012-S03 B	Mud	Piston	42.321158	-62.467133	2324	700	705	0.5	1.2	0.1	-	20.15	154	Ambient
2015-13, 700	NSPC-2015018-013-S03 B	Mud	Piston	42.360212	-62.465482	2208	698	704	0.3	0.9	0.08	-	20.3	123	Ambient
2016-15, 690	2016011-015 S04 B	Mud	Piston	42.305998	-63.243618	2050	684	694	-	-	-	-	20.05	136	Ambient
2016-17, 470	2016011-017 S03 B	Mud	Piston	42.228892	-63.117570	2315	463	468	0.3	0.9	0.04	-	20.1	232	Ambient
2016-20, 720	2016011-020 S03 B	Mud	Piston	42.304433	-62.685662	2190	718	723	0.3	0.9	0.08	-	20.95	158	Ambient
2016-22, 600	2016011-022 S03 B	Mud	Piston	42.009998	-62.814178	2822	598	603	0.4	1.0	0.09	-	20.42	95	Ambient
2016-24, 700	2016011-024 S02 B	Mud	Piston	41.878680	-62.837250	3095	695	700	0.3	0.9	0.1	-	20.04	99	Ambient
2016-25, 270	2016011-025 S01 B	Mud	Piston	42.053920	-62.518298	2880	267	272	0.3	0.8	0.05	-	21.45	132	Ambient
2016-25, 290	2016011-025 S02 B	Mud	Piston	42.053920	-62.518298	2880	287	292	0.2	0.8	0.03	-	20	375	
2016-25, 300	2016011-025 S03 B	Mud	Piston	42.053920	-62.518298	2880	301	306	0.3	0.9	0.07	-	20	280	
2016-25, 800	2016011-025 S04 B	Mud	Piston	42.053920	-62.518298	2880	791	796	0.4	1.0	0.1	-	20.16	492	
2016-26, 490	2016011-026 S02 B	Mud	Piston	42.104218	-62.538445	2760	483	488	0.4	1.0	0.07	-	20	152	Ambient
2016-28, 660	2016011-028 S02 B	Mud	Piston	42.279317	-62.310168	2510	655	660	0.3	0.9	0.09	-	20.07	229	Ambient
2016-29, 700	2016011-029 S03 B	Mud	Piston	42.196683	-62.313510	2730	704	709	0.5	1.2	0.07	-	20	421	Ambient
2016-30, 630	2016011-030 S02 B	Mud	Piston	42.470058	-62.130127	2106	630	635	0.3	0.9	0.09	-	20.17	146	Ambient
2016-49, 450	2016011-049 S06 B	Mud	Piston	42.159815	62.359747	2715	443	448	0.5	1.0	0	-	20.18	217	Ambient
2018-21, 0	2018041-0021 gc	Mud	Gravity	42.494195	-62.126415	2079	5	10	0.7	0.9	0.1	-	22.01	177	Ambient
2018-21, 60	2018041-0021 gc	Mud	Gravity	42.494195	-62.126415	2079	55	60	0.5	0.8	0.07	-	20	547	
2018-21, 140	2018041-0021 gc	Mud	Gravity	42.494195	-62.126415	2079	140	145	0.5	0.9	0.08	-	20.43	500	
2018-21, 210	2018041-0021 gc	Mud	Gravity	42.494195	-62.126415	2079	210	217	0.4	0.9	0.05	-	20.55	128	
2018-21, 240	2018041-0021 gc	Mud	Gravity	42.494195	-62.126415	2079	236	241	0.4	0.9	0.07	-	20.06	187	
2018-21, 320	2018041-0021 gc	Mud	Gravity	42.494195	-62.126415	2079	312	317	0.5	1.1	0.05	-	20.03	108	
2018-21, 410	2018041-0021 gc	Mud	Gravity	42.494195	-62.126415	2079	405	410	0.2	0.8	0.05	-	20.3	324	
2018-21, 450	2018041-0021 gc	Mud	Gravity	42.494195	-62.126415	2079	446	451	0.2	0.8	0.05	-	20.13	144	
2018-21, 520	2018041-0021 gc	Mud	Gravity	42.494195	-62.126415	2079	514	520	0.2	0.8	0.04	-	20.03	247	
2018-21, 570	2018041-0021 gc	Mud	Gravity	42.494195	-62.126415	2079	565	570	0.3	0.9	0.05	-	20.27	148	
2018-21, 610	2018041-0021 gc	Mud	Gravity	42.494195	-62.126415	2079	610	615	0.3	0.9	0.07	-	20.04	168	
2018-21, 670	2018041-0021 gc	Mud	Gravity	42.494195	-62.126415	2079	667	672	0.3	0.9	0.07	-	20.21	146	
2018-21, 710	2018041-0021 gc	Mud	Gravity	42.494195	-62.126415	2079	710	715	0.3	0.9	0.06	-	20.03	182	
2018-22, 0	2018041-0022 gc	Mud	Gravity	42.492181	-62.128928	2083	0	5	0.7	0.9	0.09	-21.74	20.05	296	Ambient
2018-22, 60	2018041-0022 gc	Mud	Gravity	42.492181	-62.128928	2083	52	60	0.6	0.9	0.08	-	20.04	504	
2018-22, 110	2018041-0022 gc	Mud	Gravity	42.492181	-62.128928	2083	110	115	0.6	1.0	0.06	-22.74	20.15	280	
2018-22, 150	2018041-0022 gc	Mud	Gravity	42.492181	-62.128928	2083	151	156	0.4	0.8	0.02	-	21.91	131	
2018-22, 270	2018041-0022 gc	Mud	Gravity	42.492181	-62.128928	2083	268	273	0.4	0.9	0.06	-23.73	20.01	125	
2018-22, 300	2018041-0022 gc	Mud	Gravity	42.492181	-62.128928	2083	301	309	0.4	1.0	0.04	-	20.5	309	
2018-22, 360	2018041-0022 gc	Mud	Gravity	42.492181	-62.128928	2083	360	365	0.4	1.0	0.07	-22.87	20.42	161	
2018-22, 410	2018041-0022 gc	Mud	Gravity	42.492181	-62.128928	2083	409	414	0.2	0.8	0.04	-23.17	20.09	141	
2018-22, 460	2018041-0022 gc	Mud	Gravity	42.492181	-62.128928	2083	460	466	0.3	0.9	0.04	-23.89	20.13	135	
2018-23, 0	2018041-0023 gc	Mud	Gravity	42.466221	-62.192356	2154	5	10	0.7	0.9	0.1	-21.77	20.02	146	Ambient
2018-23, 40	2018041-0023 gc	Mud	Gravity	42.466221	-62.192356	2154	35	40	0.6	0.9	0.09	-	20.69	192	
2018-23, 100	2018041-0023 gc	Mud	Gravity	42.466221	-62.192356	2154	92	98	0.5	0.9	0.07	-22.31	20.74	195	
2018-23, 130	2018041-0023 gc	Mud	Gravity	42.466221	-62.192356	2154	125	130	0.5	0.9	0.07	-	20.8	986	
2018-23, 200	2018041-0023 gc	Mud	Gravity	42.466221	-62.192356	2154	192	198	0.6	1.1	0.08	-22.26	20	355	
2018-23, 220	2018041-0023 gc	Mud	Gravity	42.466221	-62.192356	2154	220	225	0.7	1.2	0.08	-	20.12	242	
2018-23, 280	2018041-0023 gc	Mud	Gravity	42.466221	-62.192356	2154	272	286	0.5	1.0	0.05	-23.83	20.15	399	
2018-23, 340	2018041-0023 gc	Mud	Gravity	42.466221	-62.192356	2154	335	340	0.5	1.0	0.07	-24.38	20.09	354	
2015-16, 620	NSPC-2015018-016-S04 B	Mud	Piston	42.774882	-61.234878	2233	614	619	0.4	1.0	0.09	-	20.2	168	Ambient
2016-38, 570	2016011-038 S03 B	Mud	Piston	42.862812	-60.844940	2250	563	568	0.4	1.0	0.1	-	20.31	148	Ambient
2015-24, 600	NSPC-2015018-024-S04 B	Mud	Piston	43.340303	-59.958477	1540	594	599	1.1	1.7	0.11	-	20.9	743	Ambient
2015-29, 500	NSPC-2015018-029-S03 B	Mud	Piston	43.270203	-60.058940	1620	490	495	0.8	1.4	0.12	-	20.28	560	Ambient
2018-07, 0	2018041-0007 gc	Mud	Gravity	43.010485	-60.211696	2405	0	4	0.1	0.4	0.02	-21.97	20.15	121	Seep
2018-07, 20	2018041-0007 gc	Mud	Gravity	43.010485	-60.211696	2405	18	24	0.3	0.5	0.05	-27.43	20.08	202	
2018-07, 40	2018041-0007 gc-Isojar	Isojar	Gravity	43.010485	-60.211696	2405	26	42	0.3	0.6	0.05	-22.87	22.02	207	

[a] Cores are labelled by the year of the cruise, followed by core number, core site number.

https://doi.org/10.5194/egusphere-2025-1228
Preprint. Discussion started: 28 March 2025

[b] Sediment type is sourced from open file cruise reports (Campbell and MacDonald, 2016; Campbell, 2019; and Campbell and Normandeau, 2019).

[c] Determination of hydrocarbon input is provided by Fowler et at. (2017).

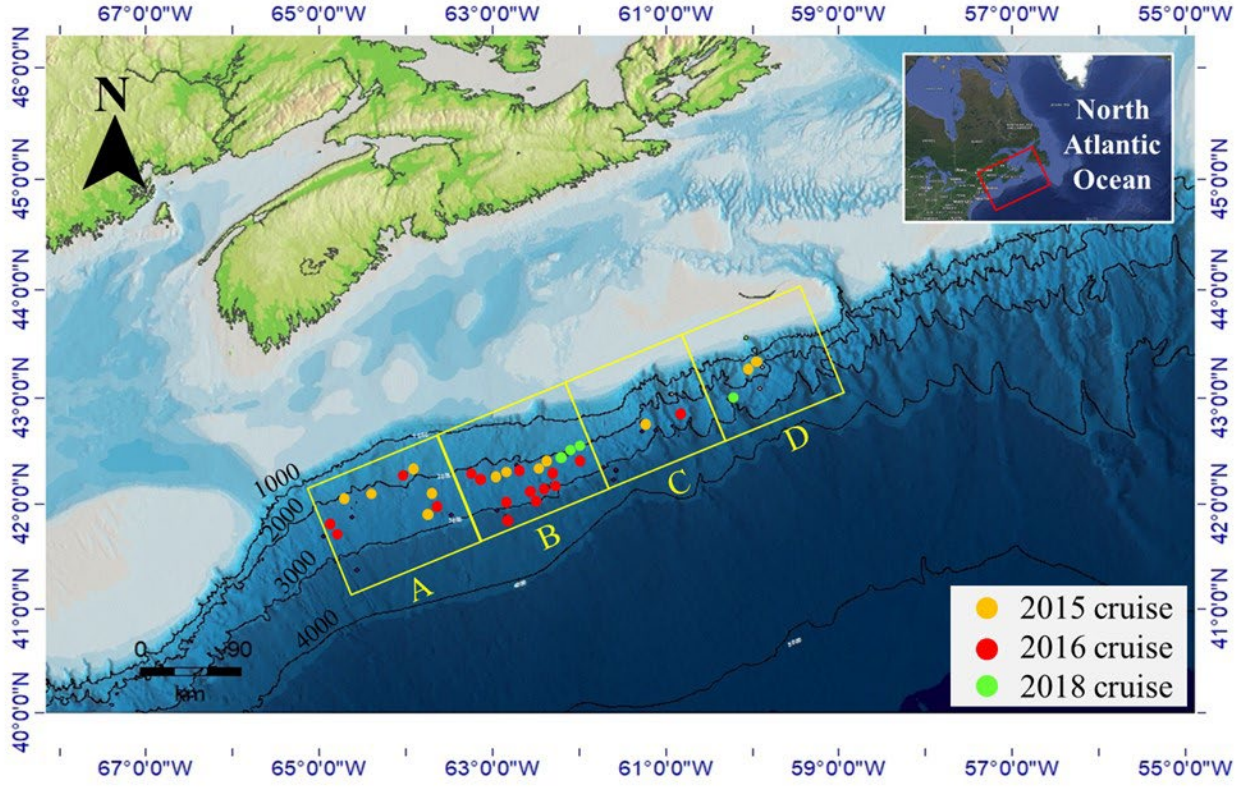

Figure 1: ArcGIS bathymetric map of the North Atlantic Scotian Margin displaying piston and gravity core locations used in this study. Core locations are grouped into four equal area quadrants (labelled A–D) that extend parallel to the Scotian Slope. Colour circles mark the year that the survey cruise was conducted.

2.3 Porewater Geochemistry

Porewater was extracted from sediments using Rhizon samplers and by centrifugation at 2500 rpm for 10 min. The porewater was decanted into a pre-combusted glass beaker, then filtered through a 0.45-µm filter to remove sediment particles. The exact volume of extracted porewater was recorded as a measure of sediment porosity. Ion chromatography is a liquid chromatographic technique that separates ions in solution based on their interaction with an ion-exchange resin within a column. A Thermo Scientific Dionex Aquion Ion Chromatography Conductivity Detector System with an anion-exchange column and a DS6 Heated Conductivity Cell fitted with an AERS_4mm suppressor pump and a Dionex AXP Auxiliary pump

https://doi.org/10.5194/egusphere-2025-1228
Preprint. Discussion started: 28 March 2025

and pump ECD from the Saint Mary's University Organic Geochemistry Laboratory (OGL). The IC was further configured with an in-line Thermo Scientific 9×24mm Dionex InGuard Ag sample prep cartridge and Thermo Scientific Dionex InGuard Na prep cartridge to facilitate trace analysis of seawater. The system was controlled via Thermo Scientific Chromeleon 7 chromatography system version 7.3 software. Seven Anion Standard II (from Sunnyvale, California) in deionized water. The anion standard (S+D) was an amalgamation of H_2O (99.9%, CAS# 7732-18-5) and the following anions – F^- (20 mg/L, CAS# 7681-49-4); Cl^- (100 mg/L, CAS# 100 mg/L); NO_2^- (100 mg/L, CAS# 7632-00-0); Br^- (100 mg/L, CAS# 7647-15-6); NO_3^- (100 mg/L, CAS# 7631-99-4); PO_4^{3-} (200 mg/L, CAS# 7778-77-0); SO_4^{2-} (100 mg/L, CAS# 7757-82-6), stored in -4 °C refrigerator. Carbonate and Sulfite are prepared as separate stock solutions. Carbonate is prepared using Anhydrous Sodium Carbonate ACS powder from Fisher Chemicals (CAS # 497-19-8) and SO_3^{2-} is prepared using Anhydrous Sodium Sulfite crystalline powder from Fisher Chemicals (CAS# 7757-83-7). A seven-anion standard mixture was diluted to 0.5, 1, 2, 5, 10, 20, and 50 ppm to generate an external calibration curve. The high salinity of marine porewater requires that the system be equipped with two in-line guard cartridges to remove chloride (Cl^-) and sodium (Na^+) ions from the sample before reaching the anion-exchange column.

2.4 Lipid extraction

Before extraction, PAF (1-alkyl-2-acetoyl-sn-glycero-3-phosphocholine) was added as a recovery standard into the samples. Total lipid extracts (TLE) were recovered with a modified Bligh and Dyer extraction technique (Bligh and Dyer, 1959; Sturt et al., 2004) following additional protocols described in Bentley et al. (2021). The liquid-liquid extraction method employed a blend of polar and non-polar solvents that effectively separates the organic phase from the inorganic phase, while gently lysing living cellular membranes.

2.5 Lipid separation and identification

Aliquots comprising 1 % and 3 % of the TLE were injected into an Agilent Technologies 1290 Infinity II ultra-high performance liquid chromatograph (UHPLC) coupled to a 6530-quadrupole time-of-flight mass spectrometer (qToF-MS) run in reverse phase using electrospray ionization. Liquid chromatographic separation used a ZORBAX RRHD Eclipse Plus C18 (2.1-mm×150-mm×1.8-µm) reverse phase column, equipped with a guard column, and maintained at a stable temperature of 45 °C throughout the sample analysis. The injection solvent was methanol. The mobile phase flow rate was set at 0.25 mL min^{-1} with the composition of mobile phases being methanol/formic acid/ammonium hydroxide ([100:0.04:0.10] v:v:v) for mobile phase A, and propan-2-ol/formic acid/ammonium hydroxide ([100:0.04:0.10] v:v:v) for mobile phase B. The mobile phase composition was 100 % A for 10 min., followed by a linear addition of B to 24 % held for 5 min., followed by a linear gradient to 65 % B for 75 min., then 70 % B for 15 min., and finally re-equilibrating with 100 % A for 15 min.

Compounds were tentatively identified by mass spectral analysis in conjunction with expected chromatographic elution patterns (Table S2) as found in the literature (e.g. Wörmer et al., 2013; Wörmer et al., 2015; Yoshinaga et al., 2011; Schouten

https://doi.org/10.5194/egusphere-2025-1228
Preprint. Discussion started: 28 March 2025

et al., 2008; Schubotz et al., 2009; Liu et al., 2012a). Lipid quantification used C_{21}-PC (1, 2-diheneicosanoyl-*sn*-glycero-3-phosphocholine) as an internal standard and was based on accurate mass detection of $[M^{\cdot}+H]^+$, $[M^{\cdot}+NH_4]^+$, and $[M^{\cdot}+Na]^+$ adducts using Agilent Technology Mass Hunter software. Lipids concentrations were then normalized to extracted sediment mass (µg g sed^{-1}) and sample TOC mass (µg wt.% TOC^{-1}).

2.6 Calculation of TOC decay rate for lipid normalization

Total organic carbon contents systematically decrease by diagenetic processes as sediments become more deeply buried. These changes result in a depth bias for lipid concentrations normalized to sediment TOC. To correct for this, the inferred TOC value at depth *i* marking the original point in time of sediment deposition ($TOC_{adjusted_i}$) was calculated as the sum of the measured TOC content in the sediment samples ($TOC_{measured_i}$) plus the TOC that is predicted to have decayed ($TOC_{decayed_i}$) following Eq. (1):

$$TOC_{adjusted_i} = TOC_{measured_i} + TOC_{decayed_i}, \quad (1)$$

The decayed TOC was inferred based on a regionalized Scotian Slope sediment TOC depth profile that extended to 8.71 mbsf as calculated from the 74 samples collected from this study as well as 11 additional shallow sediment samples (<1 m) collected from ambient sediments. The resulting diagenetic decay curve (Fig. 2 and Eq. (2))

$$y = -366.2 \ln(TOC) + 47.102, \quad (2)$$

was then used to predict a regionalized reference TOC ($TOC_{predicted}$) value for any depth (y) within the study (Eq. (3)).

$$TOC_{predicted} = e^{\frac{47.102-y}{366.2}}, \quad (3)$$

The TOC decay rate (*n*) varies with sediment depth and must be determined specifically for each 1 m burial depth interval (y) following Eq. (4):

$$f(n_i) = \frac{d(TOC_{predicted_i})}{dy_i} = -\frac{TOC_{predicted_i}}{366.2}, \quad (4)$$

$$TOC_{decayed_i} = \sum_1^i (n_i \times TOC_{predicted_{i-1}}), \quad (5)$$

where n_i is the TOC decay rate at depth *i*. The $TOC_{decayed}$ and $TOC_{adjusted}$ were then calculated at each depth using Eq. (5) and Eq. (1) respectively and following the modelled TOC decay rate in Eq. (5) Table 2, and Fig. S1.

https://doi.org/10.5194/egusphere-2025-1228
Preprint. Discussion started: 28 March 2025

Table 2: Modelled TOC decay rate and pre-diagenesis scaling values for various burial depths (Eq. (2), (4), and (5)).

y_i (mbsf)	$TOC_{predicted_i}$ (wt. %) Eq. (3)	n_i Eq. (4)	$TOC_{decayed_i}$ (wt. %) Eq. (5)
0	1.1	NA	NA
1	0.9	-0.24	0.3
2	0.7	-0.18	0.4
3	0.5	-0.14	0.5
4	0.4	-0.10	0.6
5	0.3	-0.08	0.6
6	0.2	-0.06	0.6
7	0.2	-0.05	0.6
8	0.1	-0.03	0.6
9	0.1	-0.03	0.6

2.7 Statistical analysis

A heatmap dendrogram was generated with the R statistical software environment (R Core Team, 2023) using the ggplot2 package, which allowed for the integration of the dendrogram with a color-coded matrix. Matrix cells were coloured according to a gradient scale representing the z-scored values. To assess the patterns of similarity among the lipid compounds and the sediment samples, HCA was also performed. Minitab statistical software was used to perform PCA. Diagnostic principal components were extracted using eigenvalues greater than one as the criteria and then were displayed as both factor loading and score plots.

3 Results

3.1 Bulk sedimentary organic matter

Sedimentary organic carbon ranged from 0.12 to 1.1 wt. % with an average of 0.5 wt. % (Fig. 2 and Table 1). This was calculated based on 85 TOC measurements produced from 33 sediment cores. A sharp down core decrease in TOC is observed from 0 to 0.5 mbsf, which is followed by a more gradual decrease with core depth. The TN values ranged from 0 to 0.12 wt. % with an average of 0.07 wt. % (Fig. 2 and Table 1). Samples "2016-049, 443-448 cm" and "2015-029, 490-495 cm" comprise the lowest and highest TN values, respectively. The $\delta^{13}C_{TOC}$ values range from -21.7 to -24.4 ‰ (Fig. 2 and Table 1), with one outlier of -27.4 ‰ collected from seep site (core "2018, 0007"). Collectively, these trends are consistent with typical shallow marine sediments experiencing early diagenetic alteration of its organic matter.

https://doi.org/10.5194/egusphere-2025-1228
Preprint. Discussion started: 28 March 2025

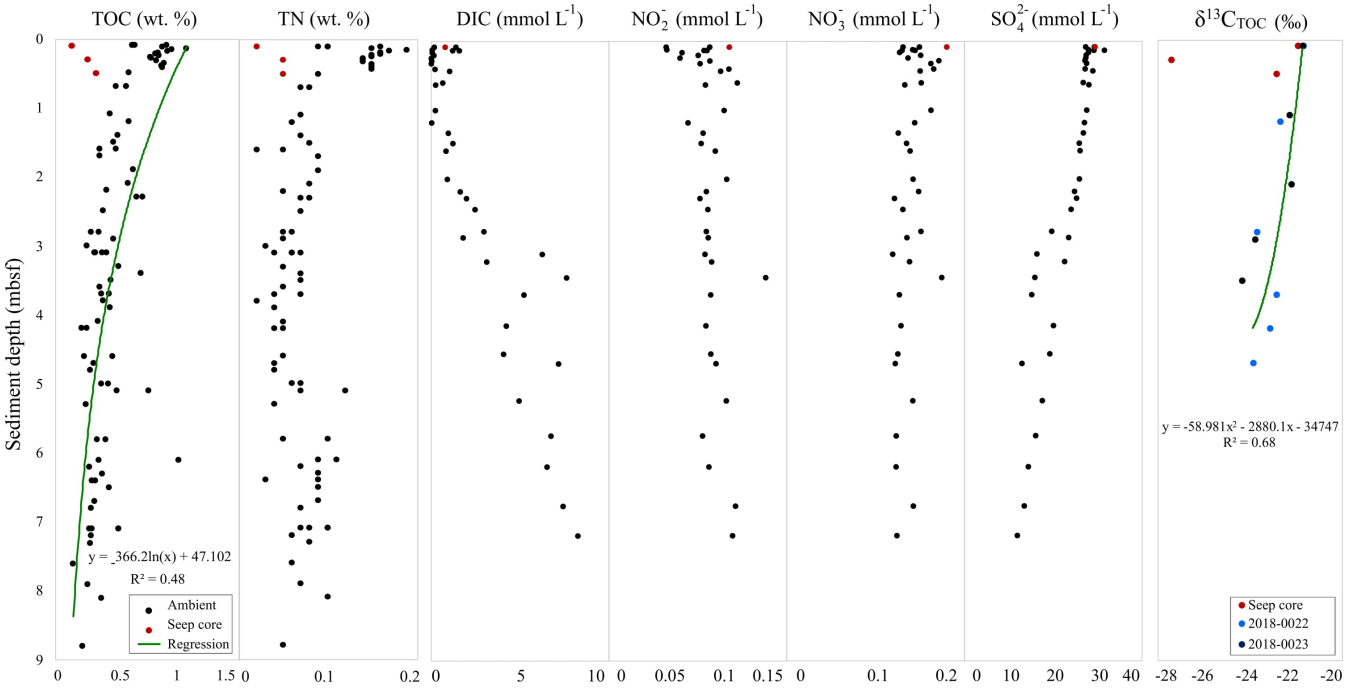

Figure 2: Down core TOC, TN, DIC, pore water anions, and stable carbon isotope ($\delta^{13}C_{TOC}$) trends of the Scotian Slope sediment samples.

220

3.2 Diversity of archaeal lipids in the Scotian Slope sediments

A total of 14 archaeal lipid classes comprising 42 unique compounds were tentatively identified and quantified across 74 sediment samples using mass spectrometric techniques and comparisons of elution times from the literature (Fig. 3 and Supplemental Tables 3 and 4). Lipid classes were grouped based on their degree of preservation into IPLs, CLs, and CL-DPs.
225 Additionally, upper water column plant-based chlorophyll-*a* (Chl-*a*) and hydroxy-chlorophyll-*a* (OH-Chl-*a*) were identified and quantified as outgroup allochthonous additions to the seafloor.

Eight IPL classes comprising 18 unique compounds were identified (Fig. 3 and Supplemental Table S4). Detected mono-glycosidic glycerol dialkyl glycerol tetraethers (1G-GDGTs) included 0–3 and crenarchaeol (Cren). For this series 1G-GDGT-0 and 1G-Cren were the most abundant compounds. For di-glycosidic GDGTs (2G-GDGTs), compound classes included 0–2
230 rings and Cren, with the acyclic lipid being the dominant compound. Detected hydroxyl mono-glycosidic glycerol dialkyl glycerol tetraether (1G-OH-GDGTs) were -0 to -2, with 1G-OH-GDGT-0 being the dominant compound. Hydroxyl di-glycosidic glycerol dialkyl glycerol tetraethers (2G-OH-GDGTs) ranged from 0–2 with the dominant compound also being 2G-OH-GDGT-0. Apart from monolayer lipid structures, four C_{40} bilayer IPLs were detected. These included mono- and di-glycosidic (1G- and 2G-ARs), phosphatidicacid, (PA-AR), and hydroxyphosphatidicacid (PA-OH-AR) archaeols.

https://doi.org/10.5194/egusphere-2025-1228
Preprint. Discussion started: 28 March 2025

Six classes of CL and CL-DPs comprising 24 unique compounds were identified (Fig. 3 and Supplemental Table S3). Commonly detected GDGTs were 0–3, Cren, and the regioisomer of Cren (Cren′). For these compounds, prevalent GDGT-0 and Cren were most abundant archaeal lipids in the surveyed region of the Scotian Slope sediments. Detected hydroxyl glycerol dialkyl glycerol tetraethers (OH-GDGTs) comprised OH-GDGT (0–3, and Cren) with OH-GDGT-0 being the dominant compound were also observed in all surveyed samples. Archaeol was detected in all sediment samples, where it typically marked the third most abundant archaeal lipid on most sediment samples (Fig. 3 and Supplemental Table 3).

Archaeal CL-DPs can take on many forms (e.g., Liu et al., 2016). For this study, only 13 derivatives were targeted. These include glycerol dialkanol diethers (GDDs) 0–4 and Cren, with GDD-0 and GDD-Cren being the dominant compounds; hydroxylated glycerol dialkanol diethers (OH-GDDs) 0–2, dominated by OH-GDD-0; and biphytanic diols 0–3 (BpDiols) with BpDiol-0 being the most prevalent highly degraded archaeal biomarker.

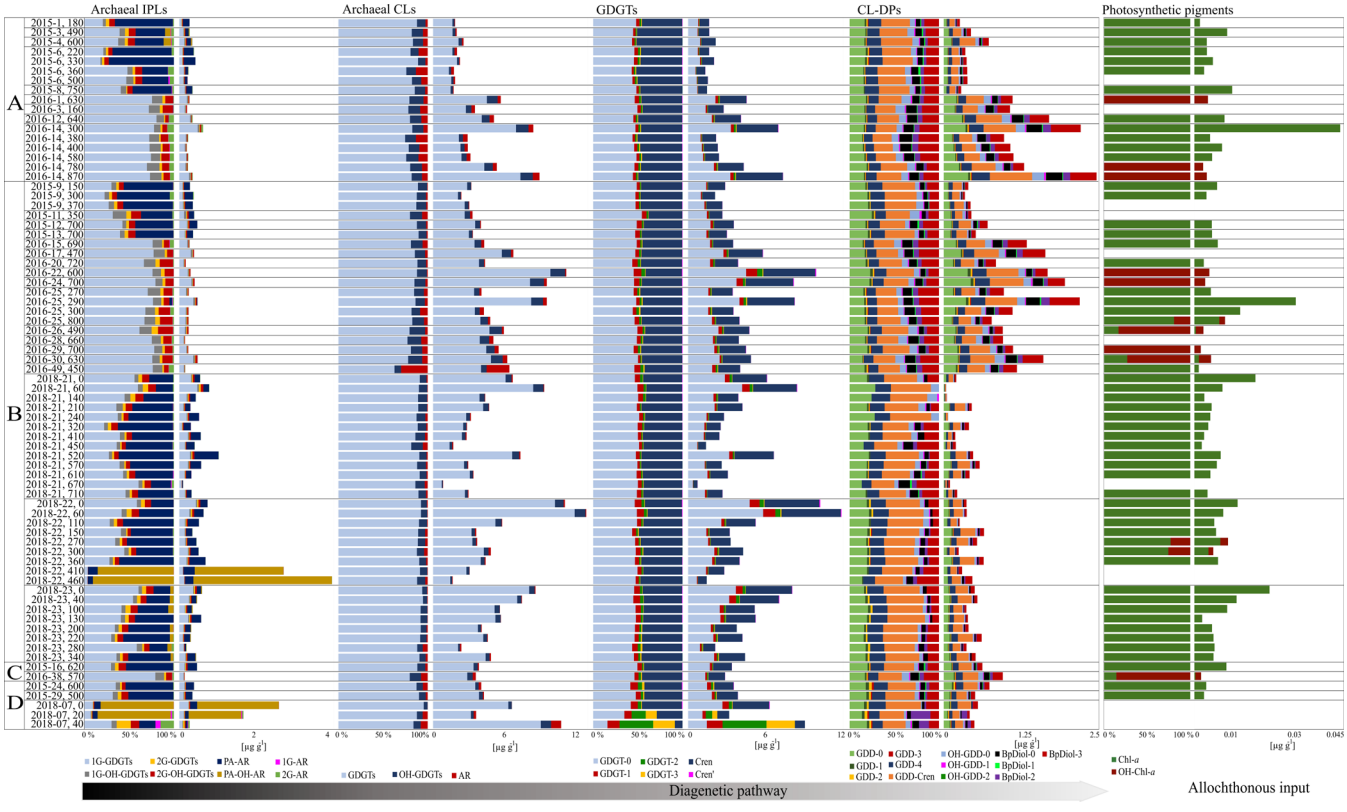

Figure 3: Relative and absolute abundances of archaeal IPL, CL, and CL-DP classes within the four quadrants (A-D), Scotian Slope (Fig. 1) sediments.

https://doi.org/10.5194/egusphere-2025-1228
Preprint. Discussion started: 28 March 2025

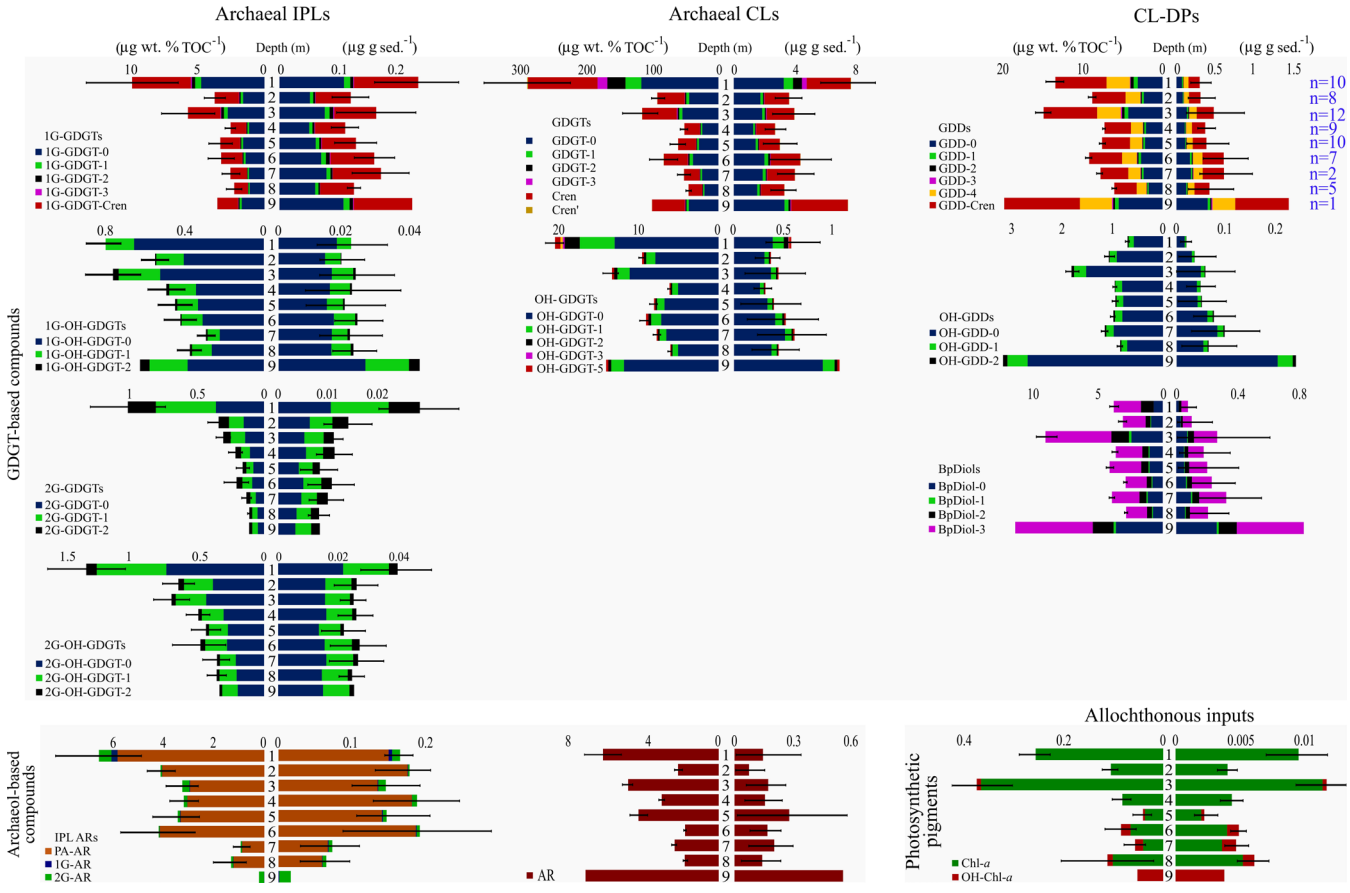

Figure 4: Bar graphs of down-core archaeal lipid class abundances normalized to sediment (right) and TOC (left) (blue font "n" indicates the summed samples for each depth interval). Black lines through the bars of each graph mark standard deviations of lipid abundance measurements.

4 Discussion

4.1 Chemotaxonomic relationships

In marine environments, isoprenoidal GDGTs are mainly derived from ammonia-oxidizing Thaumarchaeota that inhabit both the surface ocean and mesopelagic zone (Schouten et al., 2002; Church et al., 2010; Villanueva et al., 2015). The high concentration of Cren and GDGT-0 with relatively low contents of GDGT-1 to -3 and Cren´ in environmental samples are predominantly non-thermophilic Thaumarchaeota source of GDGTs (Schouten et al., 2000; Schouten et al., 2013; Schouten et al., 2002). GDGT-0 is also produced by methanogenic Euryarchaeota (Blaga et al., 2009). Similarly, Thaumarchaeota group I.1a, is an additional producer of Cren. OH-GDGTs are absent in Thaumarchaeota group I.1b, but abundant in Thaumarchaeota group I.1a (Schouten et al., 2013). Unspecified Crenarchaeota or Euryarchaeota have been proposed to synthesize OH-GDGTs

https://doi.org/10.5194/egusphere-2025-1228
Preprint. Discussion started: 28 March 2025

(Lü et al., 2015). High temperature enhances production of OH-GDGTs with a higher degree of cyclization (Lü et al., 2015; Umoh et al., 2022). GDDs are mostly regarded as degradation products of GDGTs in the environment (e.g., Mitrović et al., 2023; Hingley et al., 2024). However, IPL-based GDDs have also been detected in cultures of various methanogenic archaea, such as *Methanosarcina mazei* and *Methanosphaera stadtmanae* (Liu et al., 2012; Meador et al., 2014; Bauersachs et al., 2015), implying that GDDs are also biosynthesized by living organisms although the exact pathways have not been determined. Archaeol is synthesized by members of Euryarchaeota, Crenarchaeota, and Thaumarchaeota (Koga et al., 1993). In environmental samples, the detection of AR is mainly associated with methanogenic microorganisms (Pancost et al., 2011) and ANME (Rossel et al., 2008).

4.2 Regional sediment depth trends and inferences on archaeal lipid source inputs

To derive regional down-core depth trends lipid concentrations from sediment samples were binned into 1 m thick stratigraphic intervals. The sediment and TOC normalized concentrations of IPLs, CLs, CL-DPs, and upper water column photosynthetic pigments were then averaged across all samples falling into its specific depth interval (Fig. 4). The 14 lipid classes have distinct trends with both increasing and decreasing loadings with sediment depth that are further complicated by occasional lack of consistency between the two normalization schemes. These variations strongly suggest the lipid class are derived from different source inputs.

Resolving archaeal lipid source inputs is difficult and the subject of long-term disagreement (e.g., Zhang et al., 2011; Hu et al., 2015; Li et al., 2016; Guo et al., 2018; Cheng et al., 2021; Umoh et al., 2022;). For this study, the interpretation of lipid sourcing considers the following framework. Comparisons between the two lipid normalization methods enable a basic premise for determining allochthonous versus autochthonous input. This is because normalization by sediment TOC adjusts the lipid concentration relative to what is largely an allochthonous input of upper water column supply of detrital sedimentary organic matter. Alternatively, because the ocean floor sediments contain relatively low organic matter abundances (<1.1 wt. %) the method of normalizing lipid concentrations to sediment volume imparts little influence from upper primary productivity. Therefore, when these two normalization schemes produce similar depth trends, the quantified lipid is likely derived from the overlying water column. However, if dissimilar down core profiles are found then the lipid is more likely to have been sourced from within its host sediment. Photosynthetic pigments Chl-*a* and OH-Chl-*a* from the euphotic zone of the water column should also provide a stratigraphic record of changing productivity through time. These pigments alternate between high and low loadings and have near identical depth trends across both normalization methods (Fig. 4). We therefore interpret other lipid classes as being largely sourced from the upper water column if 1) their down-core profiles are the same across both normalization schemes and 2) their stratigraphic loadings match the measured Chl-*a* and OH-Chl-*a* depth profiles. We further interpret the lipid class as being sourced from within the sediments if the lipid normalized to TOC has a much greater trend than what is observed if it is sediment normalized.

The normalized down core profiles suggest that among the IPLs, 1G-GDGT-0, -1, and -Cren and CL GDGTs are largely dominated by upper water column inputs as their two normalized stratigraphic trends largely replicate that of the photosynthetic

https://doi.org/10.5194/egusphere-2025-1228
Preprint. Discussion started: 28 March 2025

pigments. 2G-GDGTs and 1G-OH-GDGT-0, -1, and -2 appear to be sourced from within the shallow 0-3 mbsf and the deepest 9 mbsf sediment interval as their TOC normalized abundances are largely that of the sediment normalized abundance for these intervals. IPL ARs also appear to be largely sourced from sediments as their abundances are distinctly different from that of the photosynthetic pigments down core trends. All CL GDGTs have the same relative down core depth profiles for both normalization schemes and closely match the photosynthetic pigment trends. They therefore are interpreted to be sourced from the water column. Similar to their IPL precursors, OH-GDGTs also appear to be sourced from the sediments as the compounds have more dominant TOC normalized relative to sediment normalized abundances. For CL-DPs, the larger TOC normalized contributions of GDDs, OH-GDDs, and BpDiols suggests these compounds are largely derived from within the sediments. In summary, water column loading is the main source for 1G-GDGTs in the Slope. 2G-GDGTs, OH-GDGTs, ARs, and CL-DPs have a mixed source, but largely derived from within the ocean floor sediments.

4.3 Lipidomic composition of putatively identified cold seeps

The diversity of GDGTs moieties remains consistent across the surveyed region of the slope (Fig. 3). Among our samples, sediment samples from core "2018, 0007" display a distinctively different archaeal lipid pattern, with higher levels of GDGT-2 and -3 compared to other GDGT moieties (Fig. 3). In this core, the distribution pattern of living sedimentary archaeal populations differs significantly from that of fossil lipids (CLs). That shows disparate origins for archaeal IPLs and CLs. This observation points towards complex microbial interactions and varying sedimentary processes in this specific core.

4.4 Scotian Slope archaeal lipidomes

4.4.1 Resolution of lipidomes

A heatmap dendrogram of sediment normalized lipid concentrations was calculated to resolve Scotian Slope-wide diversity patterns (Fig. 5). From this, four distinct groups of lipid classes (labelled as 1a, 1b, 1c, 2, 3, and 4) were resolved. These classes mostly arise from distinct assemblages of IPL, CL, CL-DPs, but also mark differences in water column (i.e., lipid class1a) and sediment (i.e., lipid classes 1b, 1c, 2, and 3) inputs. Additionally, six group of samples including four main groups and 3 sub-groups (labelled as lipidomes A1, A2, A3, A4.1, A4.2, and A4.3) were further identified representing complex assemblages of living, fossil, and further degraded lipids within the slope sediments. These six lipidomes have overlapping sediment depth ranges (Fig. 6).

PCA analysis was performed to further validate the heatmap dendrogram results. The first two components, which account for 85 % of the variance in the data, were selected for visualization (Fig. S3). The components were extracted using eigenvalues greater than one. The results are displayed as both factor loading and score plots. The factor loading plot (Fig. 7) yields three primary lipid clusters (labelled 1–3), with further subdivisions (labelled 1a, 1b, 2, 3a, and 3b). The score plot shows sample clusters that largely group by sediment depth (Fig. 6). Additionally, the scores plot with samples grouped by their location within the four quadrants of the Scotian Slope as outlined in Figure 1 indicates no preferential lipidomic changes along the

https://doi.org/10.5194/egusphere-2025-1228
Preprint. Discussion started: 28 March 2025

length of the slope (Fig. S4). Collectively, these data largely mirror the patterns observed in the heatmap dendrogram (Fig. 5). The agreement between the two statistical measures suggests specific lipidomic signatures are characteristic features of the deep marine sediments across the Scotian Slope.

The driver for the lipidomic stratification is not fully resolved. It was initially hypothesized that lithologic changes, such as sediment mineralogical and textural variations, were the controlling factor on archaeal community compositional changes within the shallow sediments. To track this, sedimentological observations from core logs (Table S2) were used to examining the relationship between lipidomes and lithology. In this regard, texture (suggestive of grain size changes), colour (corresponding to mineralogy and potentially redox changes), and sedimentary structures were statically compared to lipidome occurrences (Fig. S5). However, no statistical correlation and meaningful relationship between these characteristics and the stratigraphic control on archaeal lipidomes was found. Alternatively, geochemical controls do appear to influence the formation and occurrence of the archaeal lipidomes.

https://doi.org/10.5194/egusphere-2025-1228
Preprint. Discussion started: 28 March 2025

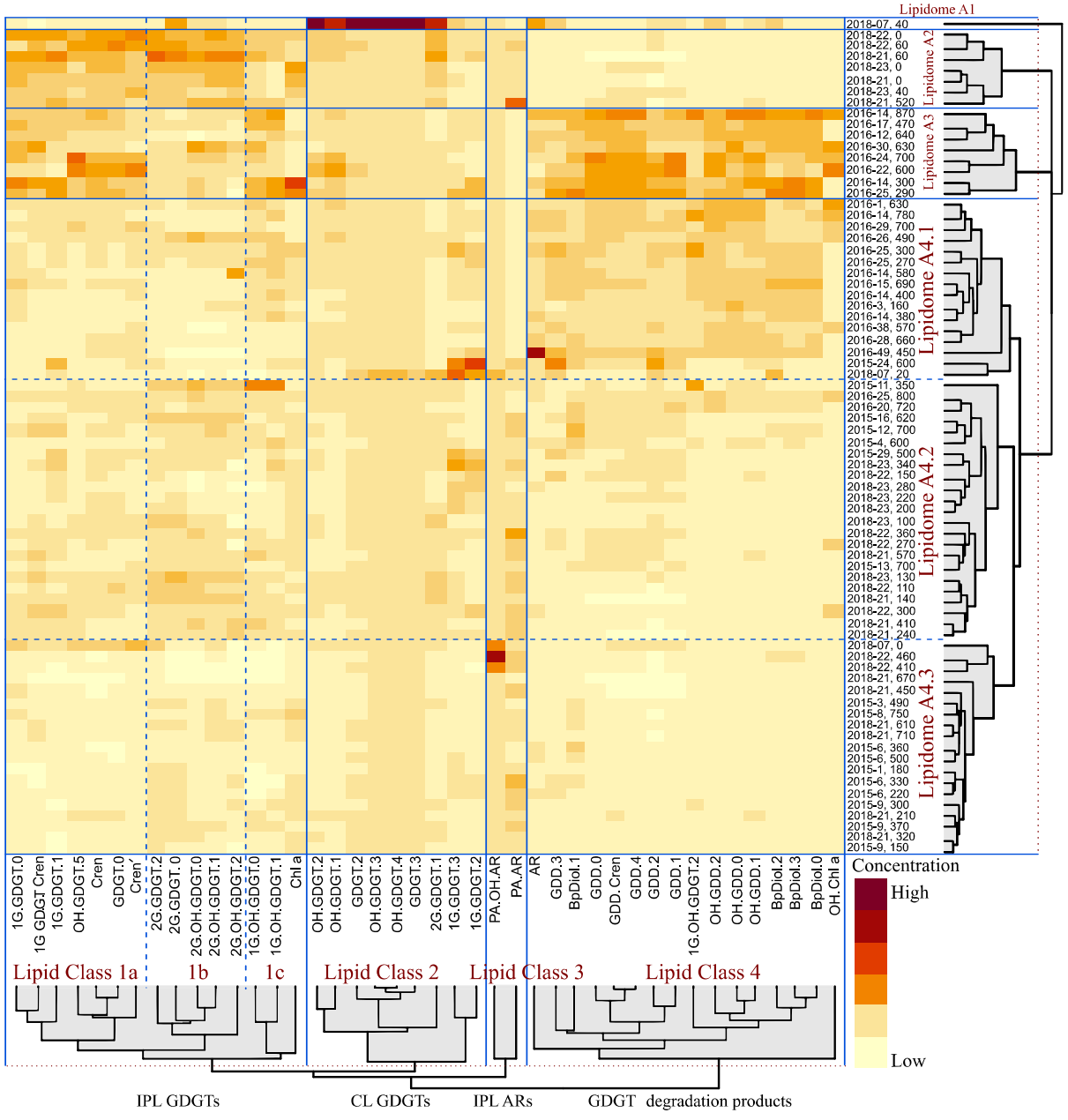

Figure 5: HCA heatmap dendrogram generated displaying the z-scored concentration of archaeal lipid compounds in the 74 sediment samples. Rows mark the individual sediment samples. Columns display normalized z-score concentrations for the different lipid compounds (with the colour gradient indicating elevated concentrations with warmer colours). Red dotted lines indicate the similarity threshold used to distinguish clusters within the HCA dendrogram. Blue dotted lines distinguish sub-groups within clusters.

https://doi.org/10.5194/egusphere-2025-1228
Preprint. Discussion started: 28 March 2025

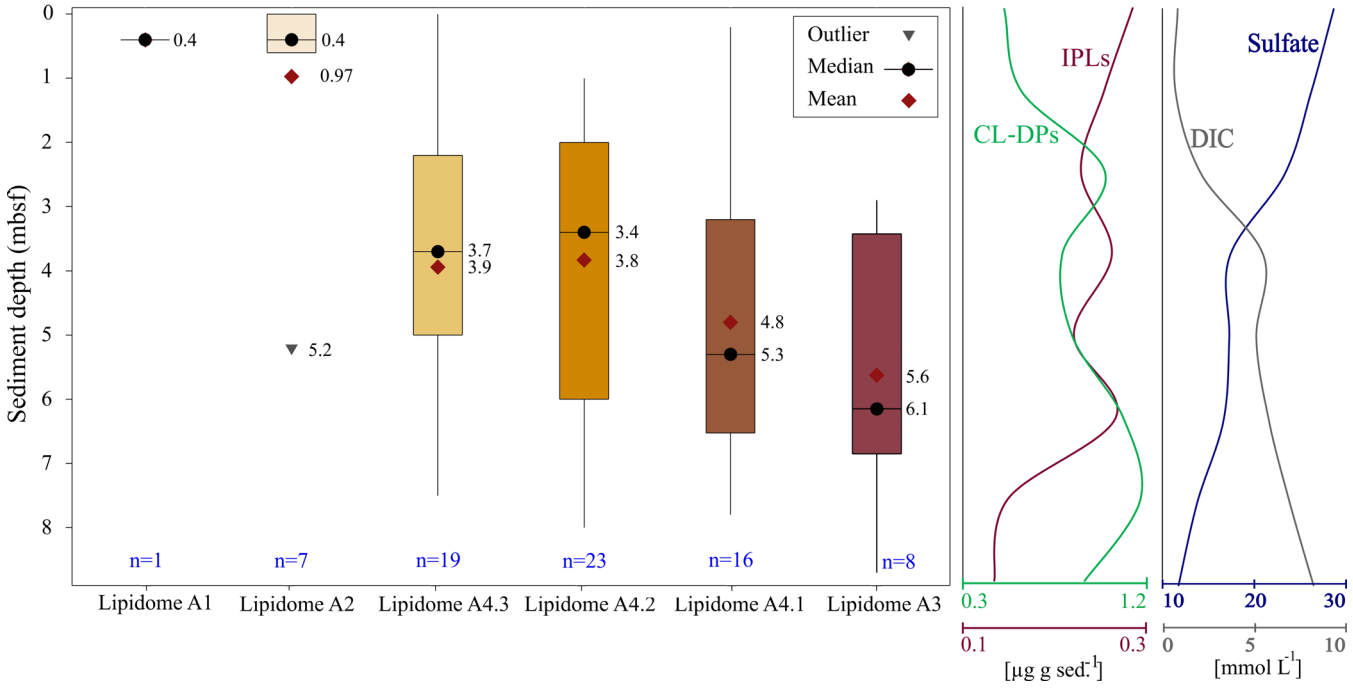

Figure 6: Box-and-whisker plot displaying the interquartile sediment burial depth ranges for six statistically defined lipidomes resolved by the heatmap dendrogram (Fig. 5), along with the smoothed down core profile showing the slope averaged concentration of IPLs, CL-DPs, sulfate and DIC made using the average concentration at 1 m depth intervals. The sulfate-alkalinity transition zone (SATZ) is labelled at the cross-over of the two down core profiles. The number of sediment samples contributing to each lipidome in the box plot is reported in blue font. The values for outlier, mean, and median refers to core depths and are in m.

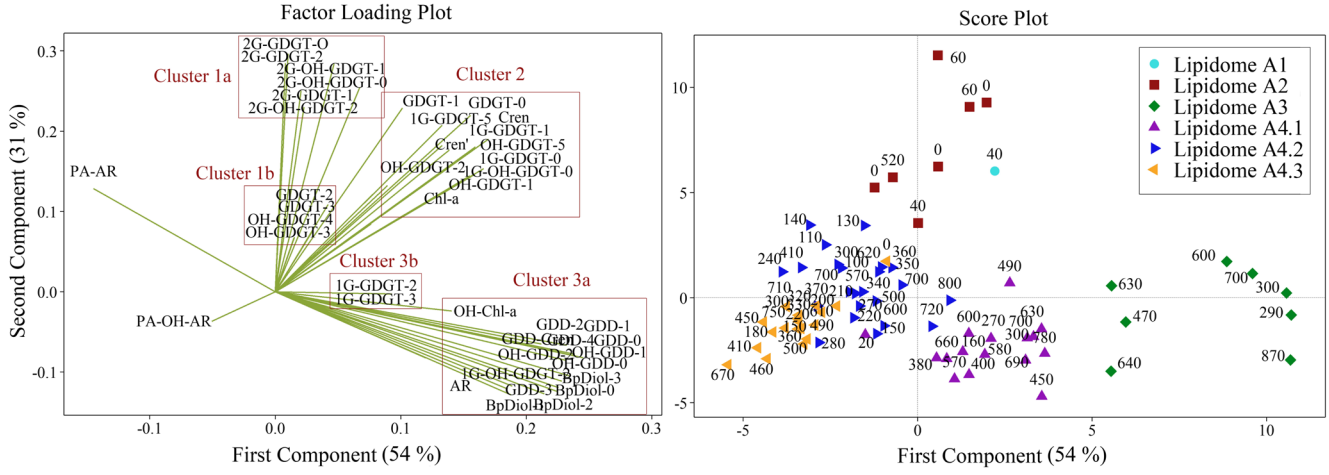

Figure 7: Principal component analysis of archaeal lipid concentrations. Factor loadings plot (left) displaying five distinct clusters. Within the score plot (right), sediment samples are grouped corresponding to the six lipidomes (numerical labels indicate the sediment burial depth of each sample in centimetres).

https://doi.org/10.5194/egusphere-2025-1228
Preprint. Discussion started: 28 March 2025

4.4.2 Microbial community reconstruction of lipidomes

The Scotian Slope's sediment depth dependent lipidomes indicate a systematic vertical change in archaeal microbial communities:

Lipidome A1 is dominated by lipid class 2 compounds, including 1G-GDGT-2, GDGT-2, 1G-GDGT-3, GDGT-3, OH-GDGT-1 to -3 as well as 2G-GDGT-0 and AR (Fig. 5), which are commonly produced by methanotrophic archaea of cold seep environments (Blumenberg et al., 2004, Pancost et al., 2001; Zhang et al., 2011). A high contribution of ANME-1 in this lipidome is shown by high concentrations of GDGT-2 and GDGT-3, in their IPL and CL forms. Thaumarchaeota group I.1a, is known to produce OH-GDGT compounds under cold, methane-rich conditions (Elling et al., 2017). Lipidome A1 includes samples whose core is associated with geochemical and microbial evidence of hydrocarbon seepage (Fowler et al., 2017).

Lipidome A2 is marked by higher concentrations of lipid classes 1a, 1b, and 1c, which includes 1G- and 2G-GDGTs, as well as GDGT-0, Cren, and Cren′ that are known to be mainly synthesized by ammonia-oxidizing Thaumarchaeota inhabiting surface and shallow sediments (Schouten et al., 2002). A strong contribution from non-thermophilic Thaumarchaeota, particularly Thaumarchaeota group I.1a in lipidome A2 is supported by high concentrations of Cren and GDGT-0 (Schouten et al., 2000, 2002, 2013).

Lipidomes A3, A4.1, and A4.3 are dominated by compounds from lipid class 4 that have higher contributions of GDGT degradation products such as GDDs, OH-GDDs, and Bp-Diols. Additionally, high concentration of Cren and GDGT-0 supports a strong contribution from non-thermophilic Thaumarchaeota in this lipidome (Schouten et al., 2000; 2002; 2013). Lipidomes A4.2 and A4.3 exhibit the lowest concentrations of archaeal lipids including GDGT degradation products (lipid class 4). These lipidomes are likely dominated by Thaumarchaeota, particularly non-thermophilic groups such as Thaumarchaeota I.1a, which produce IPLs and core GDGTs (Elling et al., 2017).

4.5 Microbial sources of GDGTs in Scotian Slope sediments

Sediments impacted by hydrocarbon seepage typically have unique microbial communities that include ANMEs (i.e., Boetius et al., 2000; Hinrichs et al., 2000; Pancost et al., 2001; Knittel and Boetius, 2009). To investigate this, down-core profiles of three archaeal lipid proxies were calculated for both CLs and IPLs to further elucidate the biogeochemical processes influencing archaeal lipid distributions within the Scotian Slope sediments (Fig. 8; Table S5). The first of these is the methane index (MI) (Eq. (6)) (Zhang et al., 2011; Guan et al., 2016). Methane-impacted sediments are usually characterized by high proportion of AMNE-1 Euryarchaeota that produce higher concentrations of GDGT-1 to -3 (Pancost et al., 2001; Blumenberg et al., 2004). MI ranges from 0 to 1 with values 0.3–0.5 indicating a transition between sediments from normal marine environments and those impacted by hydrocarbon presence (Zhang et al., 2011). MI values higher than this range indicate stronger impacts of methanotrophic communities.

$$\mathrm{MI} = \frac{[GDGT-1]+[GDGT-2]+[GDGT-3]}{[GDGT-1]+[GDGT-2]+[GDGT-3]+[Cren]+[Cren']}, \quad (1)$$

https://doi.org/10.5194/egusphere-2025-1228
Preprint. Discussion started: 28 March 2025

For the ambient sediments CL-MI values were consistently low (CLs avg. = 0.14 and IPL avg. = 0.15) across all sediment depths. IPL-MI ranged from 0.12 to 0.47; (avg. = 0.30) and systematically increase with depth, highlighting a higher proportion of AMNE-1 and -2 communities in deeper sediments. Alternatively, the hydrocarbon seep sediments of core 2018-0007 (Table 1), hosting Lipidome A1 have CL-MI have values ranging from 0.22 to 0.90; averaged at 0.56, suggesting a robust presence of methanotrophic archaea (Zhang et al., 2011; Fig. 8).

The ratios GDGT-2/Cren (Zhang et al., 2016) and GDGT-0/Cren (Blaga et al., 2009) are used to characterize methanogenic archaeal contribution to GDGT pool. GDGT-2/Cren ratios > 0.2, along with MI > 0.3, indicate methane cycling archaea (Weijers et al., 2011; Zhang et al., 2016). Ratios ranging from 0.02 to 4.37, averaging at 0.01 for ambient sediments. The seep sediments average shows a considerably higher value of 1.67. This could be indicative of an intense methane cycling process, where both methanotrophic and methanogenic activities are prominent. The sharp increase in this ratio with depth at the seep site might reflect a shift in microbial community dynamics, possibly due to increased availability of methane as an energy source in deeper layers, as noted in similar studies (e.g., Teske et al., 2018). Of additional interest is that the three proxies do not show any evidence that a vertically stratified lipidome is common to the Scotian Slope sediments. GDGT-0/Cren ratios > 2 for this ratio indicates methanogenic communities are responsible for archaeal lipid synthesis (Umoh et al., 2022). For the Scotian Slope sediments, GDGT-0/Cren ratios ranged from 0.84 to 1.86, indicating non-methanogenic contribution to archaeal pool in this system. With the exception of seep impacted sediments, all biomarker proxies indicate little activity with respect to methane cycling. Interestingly, only one of the four stratigraphically controlled lipidome of the Scotian Slope sediments is detectable by the surveyed biomarker proxies indicating CL biomarker proxies may not resolve complex changes to archaeal community structures.

https://doi.org/10.5194/egusphere-2025-1228
Preprint. Discussion started: 28 March 2025

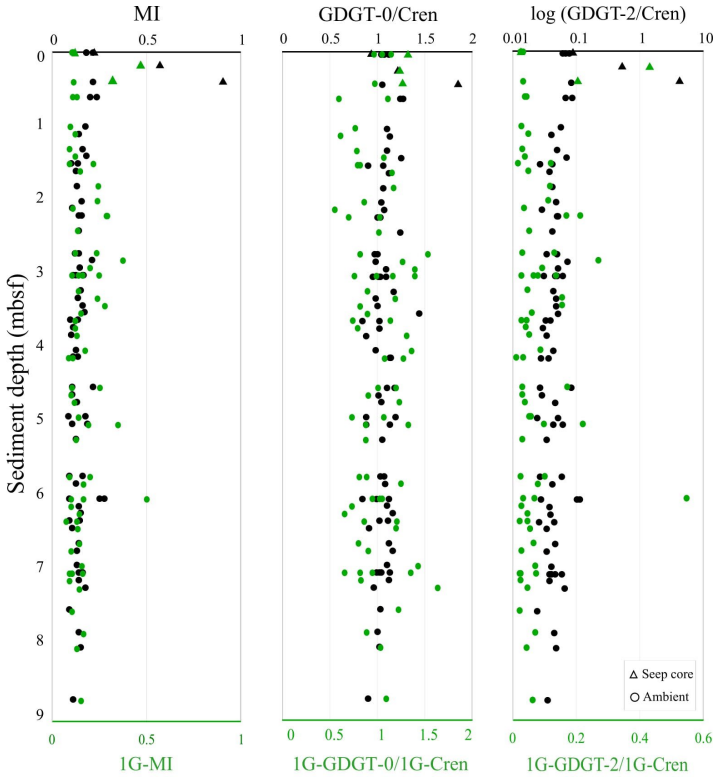

Figure 8: Down core profiles of MI, GDGT-0/Cren, and GDGT-2/Cren lipid ratios for CLs (labelled in black) and 1G-IPLs (labelled in green).

4.6 Controlling factors and the spatial extent of the Scotian Slope lipostratigraphy

Changes in sediment lithology (Fig. S5), organic matter loading (Fig. 2), methane cycling (Fig. 8) and latitudinal position along the outlined slope quadrants (Fig. 1 and Fig. S4) do not appear to fundamentally impact the lipostratigraphy. Therefore, other mechanisms must control the observed archaeal lipid diversity trends. The Scotian Slope archaeal lipidomes do however appear to be influenced by geochemical porewater changes in sulfate and DIC (Fig. 2 and 5). Lipidomes 3 and 4 occur near the sulphate alkalinity transition zone, which was determined to exist at ~3.25 mbsf (Fig. 5). This point coincides with the beginning of the lipidomes A3 and A4.1. In this regard, sediment accumulation coupled to diffusion limitation appears to be driving stratified redox controlled biogeochemical zones that are mediated and affected by partially niche-partitioned microbial habitats. Additionally, burial depth is also expected to affect the specific diagenetic pathways that impact lipid preservation. The elevated abundance of CL-DPs occurs within a sediment depth where diminishing sulfate values are reflective of elevated rates of microbial sulfate reduction. It is possible that the heterotrophic bacteria that use this metabolism may also be degrading CLs.

https://doi.org/10.5194/egusphere-2025-1228
Preprint. Discussion started: 28 March 2025

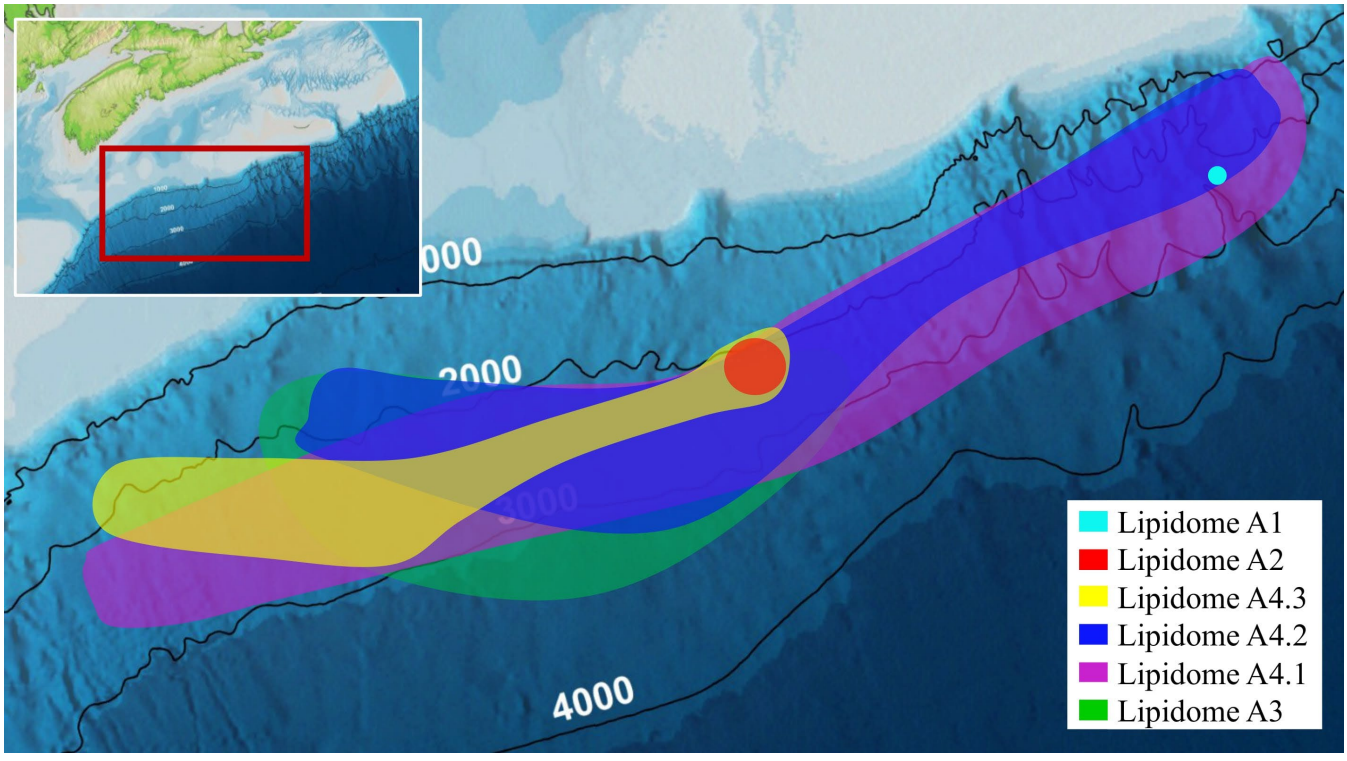

Figure 9: Scotian Slope bathymetric map showing the spatial extent of the archaeal lipostratigraphy.

5 Conclusions

This study surveyed a total of 14 archaeal lipid classes comprising 42 unique compounds tentatively identified and quantified across 74 sediment samples sourced from four equidistant quadrants of the Scotian Slope of northeast Canada that collectively covers an area ~ 40,000 km^2. The quadrants mark an ~3° of latitudinal change and transition over a water column depth that increases from ~1500 to 3500 m. The distribution of living, fossil, and degraded core lipids within the upper 9 mbsf of sediments were found to systematically vary with sediment depth forming four stratigraphically overlapping lipidomes. The lipid distributions reflect a high contribution of anaerobic methanotrophic (ANME) archaeal groups, such as ANME-1 to -3. The lipidomes appear to reflect changing microbial communities in response to hydrocarbon seepage as well as porewater geochemical changes for regions that were not impacted by seepage. A single core collected from a putative cold seep was found to have a unique lipidome composed in part by high abundances of OH-GDGTs and GDGT-2 and -3 and elevated MI values indicating higher abundances of methanotrophic Euryarchaeota. The ambient sediment lipidomes are also impacted by increasing abundances of archaeal lipid degradation products that may be a response to elevated rates of heterotrophy by microbial sulfate reducing bacteria. The three ambient sediment lipidomes appear to be highly conserved across the latitudinal

https://doi.org/10.5194/egusphere-2025-1228
Preprint. Discussion started: 28 March 2025

extent of the study area marking a resolvable shallow sediment lipostratigraphy for the Scotian Slope. The biomarker proxies measured in this study did not resolve the existing lipostratigraphy, which suggests that these techniques may miss subtle, but important, large-scale changes to the archaeal community structure within marine sedimentary systems.

Author contribution

NA and GTV designed the research and wrote the manuscript. NA generated the lipid data and provided the data analysis. UU provided technical support with lipid identification. NM provided geographical data. AM provided logistical support for sampling and project completion. ER and PG provided analytical support with bulk geochemistry and molecular analyses. MGF provided technical support for the interpretation of site localities. JNB provided technical support and helped to collect samples. VB provided technical support for porewater analysis.

Competing interests

The authors declare that they have no conflict of interest.

Acknowledgments

Thanks to the Nova Scotia Provincial Government for support of this project and spear-heading the various research cruises and surveys that made the integrative data collection possible. A special thanks is given to Carey Ryan of Net Zero Atlantic, who was the GAPP Partnership Program manager responsible for the larger group research initiatives. Carey also managed the procuration and organization of the research cruises. An additional special thanks is given to Kim Doane, the executive director of the Subsurface and Offshore Energy Branch of the Department of Energy for her support of the Organic Geochemistry Research Group at Saint Mary's University. Sediment samples analysed in this study were collected during three marine field programs led by the Geological Survey of Canada under a joint collaborative research agreement with Nova Scotian Department of Natural Resources and Renewables. Kate Jarrett of Natural Resources Canada provided the core logs that were used to describe the sediment lithologies used for the study. Nikita Lakhanpal provided porewater analyses for this study.

Financial support

Funding for this project was sourced from: Genome Atlantic and Genome Canada; Research Nova Scotia (grant no. 2142); Mitacs (grant no. IT12481 and IT29547), NetZero Atlantic and the Nova Scotia This research has been supported by the Natural Sciences and Engineering Research Council of Canada (grant no. RGPIN-2018-06147; NSERC), NSERC Canada

https://doi.org/10.5194/egusphere-2025-1228
Preprint. Discussion started: 28 March 2025

Research Chairs (CRC) program, Canada Foundation for Innovation (CFI; JELF–CRC, John R. Evans Leaders Fund), NSERC Discovery Grants program (application no. RGPIN-2017-05822).

References

Bauersachs, T., Weidenbach, K., Schmitz, R. A., and Schwark, L.: Distribution of glycerol ether lipids in halophilic, methanogenic and hyperthermophilic archaea, Organic Geochemistry, 83–84, 101–108, https://doi.org/10.1016/j.orggeochem.2015.03.009, 2015.

Bechtel, A., Smittenberg, R. H., Bernasconi, S. M., and Schubert, C. J.: Distribution of branched and isoprenoid tetraether lipids in an oligotrophic and a eutrophic Swiss lake: Insights into sources and GDGT-based proxies, Organic Geochemistry, 41, 822–832, https://doi.org/10.1016/j.orggeochem.2010.04.022, 2010.

Bentley, J. N., Ventura, G. T., Walters, C. C., Sievert, S. M., and Seewald, J. S.: The influence of near surface sediment hydrothermalism on the TEX_{86} tetraether lipid-based proxy and a new correction for ocean bottom lipid overprinting, https://doi.org/10.5194/bg-2021-245, 18 November 2021.

Biddle, J. F., Lipp, J. S., Lever, M. A., Lloyd, K. G., Sørensen, K. B., Anderson, R., Fredricks, H. F., Elvert, M., Kelly, T. J., Schrag, D. P., Sogin, M. L., Brenchley, J. E., Teske, A., House, C. H., and Hinrichs, K.-U.: Heterotrophic Archaea dominate sedimentary subsurface ecosystems off Peru, Proc. Natl. Acad. Sci. U.S.A., 103, 3846–3851, https://doi.org/10.1073/pnas.0600035103, 2006.

Blaga, C. I., Reichart, G.-J., Heiri, O., and Sinninghe Damsté, J. S.: Tetraether membrane lipid distributions in water-column particulate matter and sediments: a study of 47 European lakes along a north–south transect, J Paleolimnol, 41, 523–540, https://doi.org/10.1007/s10933-008-9242-2, 2009.

Bligh, E. G. and Dyer, W. J.: A Rapid method of total lipid extraction and purification, Canadian Journal of Biochemistry and Physiology, 37, 911–917, 1959.

Blumenberg, M., Seifert, R., Reitner, J., Pape, T., and Michaelis, W.: Membrane lipid patterns typify distinct anaerobic methanotrophic consortia, Proc. Natl. Acad. Sci. U.S.A., 101, 11111–11116, https://doi.org/10.1073/pnas.0401188101, 2004.

Boetius, A., Ravenschlag, K., Schubert, C. J., Rickert, D., Widdel, F., Gieseke, A., Amann, R., Jørgensen, B. B., Witte, U., and Pfannkuche, O.: A marine microbial consortium apparently mediating anaerobic oxidation of methane, Nature, 407, 623–626, https://doi.org/10.1038/35036572, 2000.

Burdige, D. J.: Preservation of Organic Matter in Marine Sediments: Controls, Mechanisms, and an Imbalance in Sediment Organic Carbon Budgets?, Chem. Rev., 107, 467–485, https://doi.org/10.1021/cr050347q, 2007.

Campbell, D. C.: CCGS Hudson Expedition 2016-011, phase 2. Cold seep investigations on the Scotian Slope, offshore Nova Scotia, June 15-July 6, 2016, https://doi.org/10.4095/313603, 2019.

Campbell, D. C. and MacDonald, A. W. A.: CCGS Hudson Expedition 2015-018, geological investigation of potential seabed seeps along the Scotian Slope, June 25-July 9, 2015, https://doi.org/10.4095/299390, 2016.

https://doi.org/10.5194/egusphere-2025-1228
Preprint. Discussion started: 28 March 2025

Campbell, D. C. and Normandeau, A.: CCGS Hudson Expedition 2018-041: high-resolution investigation of deep-water seabed seeps and landslides along the Scotian Slope, offshore Nova Scotia, May 26 - June 15, 2018, https://doi.org/10.4095/314695, 2019.

Cheng, Z., Yu, F., Ruan, X., Cheng, P., Chen, N., Tao, S., Zong, Y., Yang, H., and Huang, Z.: GDGTs as indicators for organic-matter sources in a small subtropical river-estuary system, Organic Geochemistry, 153, 104180, https://doi.org/10.1016/j.orggeochem.2021.104180, 2021.

Church, M. J., Wai, B., Karl, D. M., and DeLong, E. F.: Abundances of crenarchaeal *amoA* genes and transcripts in the Pacific Ocean, Environmental Microbiology, 12, 679–688, https://doi.org/10.1111/j.1462-2920.2009.02108.x, 2010.

Deptuck, M. E. and Kendell, K. L. A Review of Mesozoic-Cenozoic Salt Tectonics Along the Scotian Margin, Eastern Canada. In J. Soto, J. F. Flinch, and G. Tari (Eds.), Permo-Triassic Salt Provinces of Europe, North Africa, and the Atlantic Margins (Ch. 13, pp. 287-312). Amsterdam, Netherlands: Elsevier, 2017.

Deptuck, M. E. and Kendell, K. L. Atlas of 3D seismic surfaces and thickness maps, central and southwestern Scotian Slope. Canada-Nova Scotia Offshore Petroleum Board, Geoscience Open File Report 2020-002MF – 2020-006MF, 1–51, 2020.

De Rosa, M.: Archaeal lipids: structural features and supramolecular organization, Thin Solid Films, 284–285, 13–17, https://doi.org/10.1016/S0040-6090(96)08832-3, 1996.

Dong, X., Rattray, J. E., Campbell, D. C., Webb, J., Chakraborty, A., Adebayo, O., Matthews, S., Li, C., Fowler, M., Morrison, N. M., MacDonald, A., Groves, R. A., Lewis, I. A., Wang, S. H., Mayumi, D., Greening, C., and Hubert, C. R. J.: Thermogenic hydrocarbon biodegradation by diverse depth-stratified microbial populations at a Scotian Basin cold seep, Nat Commun, 11, 5825, https://doi.org/10.1038/s41467-020-19648-2, 2020.

Elling, F. J., Könneke, M., Nicol, G. W., Stieglmeier, M., Bayer, B., Spieck, E., de la Torre, J. R., Becker, K. W., Thomm, M., Prosser, J. I., Herndl, G. J., Schleper, C., & Hinrichs, K.-U.: Chemotaxonomic characterisation of the thaumarchaeal lipidome. Environmental Microbiology, 19(7), 2681–2700. https://doi.org/10.1111/1462-2920.13759, 2017.

Fowler, M., Webb, J., Olsen, H., Ashraf, F., and Guldbrandsen, S.: Geochemistry data report for 2016 Scotian Slope piston coring program, 2017.

Fredricks, H. F. and Hinrichs, K.-U.: Proceedings of the Ocean Drilling Program, 207 Scientific Results, Ocean Drilling Program, https://doi.org/10.2973/odp.proc.sr.207.2007, 2007.

Gittins, D. A., Desiage, P.-A., Morrison, N., Rattray, J. E., Bhatnagar, S., Chakraborty, A., Zorz, J., Li, C., Horanszky, O., Cramm, M. A., Bisiach, F., Bennett, R., Webb, J., MacDonald, A., Fowler, M., Campbell, D. C., and Hubert, C. R. J.: Geological processes mediate a microbial dispersal loop in the deep biosphere, Sci. Adv., 8, eabn3485, https://doi.org/10.1126/sciadv.abn3485, 2022.

Guan, H., Feng, D., Wu, N., and Chen, D.: Methane seepage intensities traced by biomarker patterns in authigenic carbonates from the South China Sea, Organic Geochemistry, 91, 109–119, https://doi.org/10.1016/j.orggeochem.2015.11.007, 2016.

Guldbrandsen, S., Austnes, L.-K., Ashraf, F., Fowler, M., and Webb, J.: Geochemistry Data Report for 2018 Scotian Slope Coring Program, 2018.

https://doi.org/10.5194/egusphere-2025-1228
Preprint. Discussion started: 28 March 2025

Guo, W., Xie, W., Li, X., Wang, P., Hu, A., and Zhang, C. L.: Environmental factors shaping the archaeal community structure and ether lipid distribution in a subtropic river and estuary, China, Appl Microbiol Biotechnol, 102, 461–474, https://doi.org/10.1007/s00253-017-8595-8, 2018.

Harvey, H. R., Fallon, R. D., and Patton, J. S.: The effect of organic matter and oxygen on the degradation of bacterial membrane lipids in marine sediments, Geochimica et Cosmochimica Acta, 50, 795–804, https://doi.org/10.1016/0016-7037(86)90355-8, 1986.

Harvey, H. R., Tuttle, J. H., and Tyler Bell, J.: Kinetics of phytoplankton decay during simulated sedimentation: Changes in biochemical composition and microbial activity under oxic and anoxic conditions, Geochimica et Cosmochimica Acta, 59, 3367–3377, https://doi.org/10.1016/0016-7037(95)00217-N, 1995.

Hedges, J. I. and Keil, R. G.: Sedimentary organic matter preservation: an assessment and speculative synthesis, Marine Chemistry, 49, 81–115, https://doi.org/10.1016/0304-4203(95)00008-F, 1995.

Hinrichs, K.-U. and Boetius, A.: The Anaerobic Oxidation of Methane: New Insights in Microbial Ecology and Biogeochemistry, in: Ocean Margin Systems, edited by: Wefer, G., Billett, D., Hebbeln, D., Jørgensen, B. B., Schlüter, M., and Van Weering, T. C. E., Springer Berlin Heidelberg, Berlin, Heidelberg, 457–477, https://doi.org/10.1007/978-3-662-05127-6_28, 2002.

Hingley, J.S., Martins, C.C., Walker-Trivett, C., Adams, J.K., Naeher, S., Häggi, C., Feakins, S.J., Naafs, B.D.A.: The global distribution of Isoprenoidal Glycerol Dialkyl Diethers (isoGDDs) is consistent with a predominant degradation origin, Organic Geochemistry, 192, 104782, https://doi.org/10.1016/j.orggeochem.2024.104782, 2024.

Hinrichs, K.-U., Summons, R. E., Orphan, V., Sylva, S. P., and Hayes, J. M.: Molecular and isotopic analysis of anaerobic methane-oxidizing communities in marine sediments, Organic Geochemistry, 31, 1685–1701, https://doi.org/10.1016/S0146-6380(00)00106-6, 2000.

Hoshino, T., Doi, H., Uramoto, G.-I., Wörmer, L., Adhikari, R. R., Xiao, N., Morono, Y., D'Hondt, S., Hinrichs, K.-U., and Inagaki, F.: Global diversity of microbial communities in marine sediment, Proc. Natl. Acad. Sci. U.S.A., 117, 27587–27597, https://doi.org/10.1073/pnas.1919139117, 2020.

Hu, A., Hou, L., and Yu, C.-P.: Biogeography of Planktonic and Benthic Archaeal Communities in a Subtropical Eutrophic Estuary of China, Microb Ecol, 70, 322–335, https://doi.org/10.1007/s00248-015-0597-4, 2015.

Jenner, K A, D C Campbell, J M Barnett, J Higgins, and A Normandeau. "Piston Cores and Supporting High-Resolution Seismic Data, CCGS Hudson Expedition 2015018, Scotian Slope, Offshore Nova Scotia, Canada," 2022. https://doi.org/10.4095/330088.

Joye, S. B., Bowles, M. W., and Ziervogel, K.: Marine Biogeochemical Cycles, in: The Marine Microbiome, vol. 3, edited by: Stal, L. J. and Cretoiu, M. S., Springer International Publishing, Cham, 623–671, https://doi.org/10.1007/978-3-030-90383-1_15, 2022.

Kim, J.-H., Van Der Meer, J., Schouten, S., Helmke, P., Willmott, V., Sangiorgi, F., Koç, N., Hopmans, E. C., and Damsté, J. S. S.: New indices and calibrations derived from the distribution of crenarchaeal isoprenoid tetraether lipids: Implications for

https://doi.org/10.5194/egusphere-2025-1228
Preprint. Discussion started: 28 March 2025

past sea surface temperature reconstructions, Geochimica et Cosmochimica Acta, 74, 4639–4654, https://doi.org/10.1016/j.gca.2010.05.027, 2010.

Knittel, K. and Boetius, A.: Anaerobic Oxidation of Methane: Progress with an Unknown Process, Annu. Rev. Microbiol., 63, 311–334, https://doi.org/10.1146/annurev.micro.61.080706.093130, 2009.

Koelmel, J. P., Napolitano, M. P., Ulmer, C. Z., Vasiliou, V., Garrett, T. J., Yost, R. A., Prasad, M. N. V., Godri Pollitt, K. J., and Bowden, J. A.: Environmental lipidomics: understanding the response of organisms and ecosystems to a changing world, Metabolomics, 16, 56, https://doi.org/10.1007/s11306-020-01665-3, 2020.

Koga, Y., Nishihara, M., Morii, H., and Akagawa-Matsushita, M.: Ether Polar Lipids of Methanogenic Bacteria: Structures, Comparative Aspects, and Biosyntheses, 57, 1993.

Li, C., Adebayo, O., Ferguson, D. K., Wang, S., Rattray, J. E., Fowler, M., Webb, J., Campbell, C., Morrison, N., MacDonald, A., and Hubert, C. R. J.: Bacterial anomalies associated with deep sea hydrocarbon seepage along the Scotian Slope, Deep Sea Research Part I: Oceanographic Research Papers, 193, 103955, https://doi.org/10.1016/j.dsr.2022.103955, 2023.

Li, J., Pancost, R. D., Naafs, B. D. A., Yang, H., Zhao, C., and Xie, S.: Distribution of glycerol dialkyl glycerol tetraether (GDGT) lipids in a hypersaline lake system, Organic Geochemistry, 99, 113–124, https://doi.org/10.1016/j.orggeochem.2016.06.007, 2016.

Lipp, J. S. and Hinrichs, K.-U.: Structural diversity and fate of intact polar lipids in marine sediments, Geochimica et Cosmochimica Acta, 73, 6816–6833, https://doi.org/10.1016/j.gca.2009.08.003, 2009.

Lipp, J. S., Morono, Y., Inagaki, F., and Hinrichs, K.-U.: Significant contribution of Archaea to extant biomass in marine subsurface sediments, Nature, 454, 991–994, https://doi.org/10.1038/nature07174, 2008.

Liu, X., Summons, R. E., and Hinrichs, K.: Extending the known range of glycerol ether lipids in the environment: structural assignments based on tandem mass spectral fragmentation patterns, Rapid Comm Mass Spectrometry, 26, 2295–2302, https://doi.org/10.1002/rcm.6355, 2012a.

Liu, X.-L., Lipp, J. S., Schröder, J. M., Summons, R. E., and Hinrichs, K.-U.: Isoprenoid glycerol dialkanol diethers: A series of novel archaeal lipids in marine sediments, Organic Geochemistry, 43, 50–55, https://doi.org/10.1016/j.orggeochem.2011.11.002, 2012b.

Liu, X.-L., Birgel, D., Elling, F. J., Sutton, P. A., Lipp, J. S., Zhu, R., Zhang, C., Könneke, M., Peckmann, J., Rowland, S. J., Summons, R. E., and Hinrichs, K.-U.: From ether to acid: A plausible degradation pathway of glycerol dialkyl glycerol tetraethers, Geochimica et Cosmochimica Acta, 183, 138–152, https://doi.org/10.1016/j.gca.2016.04.016, 2016.

Liu, X.-L., Lipp, J. S., Simpson, J. H., Lin, Y.-S., Summons, R. E., and Hinrichs, K.-U.: Mono- and dihydroxyl glycerol dibiphytanyl glycerol tetraethers in marine sediments: Identification of both core and intact polar lipid forms, Geochimica et Cosmochimica Acta, 89, 102–115, https://doi.org/10.1016/j.gca.2012.04.053, 07/2012a.

Lü, X., Liu, X.-L., Elling, F. J., Yang, H., Xie, S., Song, J., Li, X., Yuan, H., Li, N., and Hinrichs, K.-U.: Hydroxylated isoprenoid GDGTs in Chinese coastal seas and their potential as a paleotemperature proxy for mid-to-low latitude marginal seas, Organic Geochemistry, 89–90, 31–43, https://doi.org/10.1016/j.orggeochem.2015.10.004, 2015.

https://doi.org/10.5194/egusphere-2025-1228
Preprint. Discussion started: 28 March 2025

Meador, T. B., Zhu, C., Elling, F. J., Könneke, M., and Hinrichs, K.-U.: Identification of isoprenoid glycosidic glycerol dibiphytanol diethers and indications for their biosynthetic origin, Organic Geochemistry, 69, 70–75, https://doi.org/10.1016/j.orggeochem.2014.02.005, 2014.

Middelburg, J. J.: Marine Carbon Biogeochemistry: A Primer for Earth System Scientists, Springer International Publishing, Cham, https://doi.org/10.1007/978-3-030-10822-9, 2019.

Milenković, S. M., Zvezdanović, J. B., Anđelković, T. D., and Marković, D. Z.: The identification of chlorophyll and its derivatives in the pigment mixtures: HPLC-chromatography, visible and mass spectroscopy studies, Advanced technologies, 2012.

Mitrović, D., Hopmans, E. C., Bale, N. J., Richter, N., Amaral-Zettler, L. A., Baxter, A. J., Peterse, F., Raposeiro, P. M., Gonçalves, V., Costa, A. C., Schouten, S., Isoprenoidal GDGTs and GDDs associated with anoxic lacustrine environments, Organic Geochemistry, 178, https://doi.org/10.1016/j.orggeochem.2023.104582, 2023.

Offre, P., Spang, A., and Schleper, C.: Archaea in Biogeochemical Cycles, Annu. Rev. Microbiol., 67, 437–457, https://doi.org/10.1146/annurev-micro-092412-155614, 2013.

Orcutt, B. N., Sylvan, J. B., Knab, N. J., and Edwards, K. J.: Microbial Ecology of the Dark Ocean above, at, and below the Seafloor, Microbiol Mol Biol Rev, 75, 361–422, https://doi.org/10.1128/MMBR.00039-10, 2011.

Pancost, R. D., Hopmans, E. C., and Sinninghe Damsté, J. S.: Archaeal lipids in Mediterranean cold seeps: molecular proxies for anaerobic methane oxidation, Geochimica et Cosmochimica Acta, 65, 1611–1627, https://doi.org/10.1016/S0016-7037(00)00562-7, 2001.

Pancost, R. D., McClymont, E. L., Bingham, E. M., Roberts, Z., Charman, D. J., Hornibrook, E. R. C., Blundell, A., Chambers, F. M., Lim, K. L. H., and Evershed, R. P.: Archaeol as a methanogen biomarker in ombrotrophic bogs, Organic Geochemistry, 42, 1279–1287, https://doi.org/10.1016/j.orggeochem.2011.07.003, 2011.

Rattray, J. E., Elizondo, G., Sloan, K., Morrison, N., Fowler, M., Gittins, D. A., Webb, J., Calvin Campbell, D., MacDonald, A., and Hubert, C. R. J.: Elevated bacterial endospores associated with thermogenic hydrocarbon seeps in deep sea sediments, Organic Geochemistry, 177, 104568, https://doi.org/10.1016/j.orggeochem.2023.104568, 2023.

Rossel, P. E., Lipp, J. S., Fredricks, H. F., Arnds, J., Boetius, A., Elvert, M., and Hinrichs, K.-U.: Intact polar lipids of anaerobic methanotrophic archaea and associated bacteria, Organic Geochemistry, 39, 992–999, https://doi.org/10.1016/j.orggeochem.2008.02.021, 2008.

Schouten, S., Hopmans, E. C., Pancost, R. D., and Damsté, J. S. S.: Widespread occurrence of structurally diverse tetraether membrane lipids: Evidence for the ubiquitous presence of low-temperature relatives of hyperthermophiles, Proc. Natl. Acad. Sci. U.S.A., 97, 14421–14426, https://doi.org/10.1073/pnas.97.26.14421, 2000.

Schouten, S., Hopmans, E. C., Schefuß, E., and Sinninghe Damsté, J. S.: Distributional variations in marine crenarchaeotal membrane lipids: a new tool for reconstructing ancient sea water temperatures?, Earth and Planetary Science Letters, 204, 265–274, https://doi.org/10.1016/S0012-821X(02)00979-2, 2002.

https://doi.org/10.5194/egusphere-2025-1228
Preprint. Discussion started: 28 March 2025

Schouten, S., Baas, M., Hopmans, E. C., and Sinninghe Damsté, J. S.: An unusual isoprenoid tetraether lipid in marine and lacustrine sediments, Organic Geochemistry, 39, 1033–1038, https://doi.org/10.1016/j.orggeochem.2008.01.019, 2008.

Schouten, S., Middelburg, J. J., Hopmans, E. C., and Sinninghe Damsté, J. S.: Fossilization and degradation of intact polar lipids in deep subsurface sediments: A theoretical approach, Geochimica et Cosmochimica Acta, 74, 3806–3814, https://doi.org/10.1016/j.gca.2010.03.029, 2010.

Schouten, S., Hopmans, E. C., and Sinninghe Damsté, J. S.: The organic geochemistry of glycerol dialkyl glycerol tetraether lipids: A review, Organic Geochemistry, 54, 19–61, https://doi.org/10.1016/j.orggeochem.2012.09.006, 2013.

Schubotz, F., Wakeham, S. G., Lipp, J. S., Fredricks, H. F., and Hinrichs, K.: Detection of microbial biomass by intact polar membrane lipid analysis in the water column and surface sediments of the Black Sea, Environmental Microbiology, 11, 2720–2734, https://doi.org/10.1111/j.1462-2920.2009.01999.x, 2009.

Sinninghe Damsté, J. S., Schouten, S., Hopmans, E. C., Van Duin, A. C. T., and Geenevasen, J. A. J.: Crenarchaeol, Journal of Lipid Research, 43, 1641–1651, https://doi.org/10.1194/jlr.M200148-JLR200, 2002.

Sollich, M., Yoshinaga, M. Y., Häusler, S., Price, R. E., Hinrichs, K.-U., and Bühring, S. I.: Heat Stress Dictates Microbial Lipid Composition along a Thermal Gradient in Marine Sediments, Front. Microbiol., 8, 1550, https://doi.org/10.3389/fmicb.2017.01550, 2017.

Sturt, H. F., Summons, R. E., Smith, K., Elvert, M., and Hinrichs, K.: Intact polar membrane lipids in prokaryotes and sediments deciphered by high-performance liquid chromatography/electrospray ionization multistage mass spectrometry—new biomarkers for biogeochemistry and microbial ecology, Rapid Comm Mass Spectrometry, 18, 617–628, https://doi.org/10.1002/rcm.1378, 2004.

Teske, A., Lizarralde, D., and Höfig, T. W.: Expedition 385 Scientific Prospectus: Guaymas Basin Tectonics and Biosphere: feedbacks between continental rifting, magmatism, sedimentation, thermal alteration of organic matter, and microbial activity, International Ocean Discovery Program, https://doi.org/10.14379/iodp.sp.385.2018, 2018.

Umoh, U. U., Li, L., Wang, J., Kauluma, N., Asuquo, F. E., and Akpan, E. R.: Glycerol dialkyl glycerol tetraether signatures in tropical mesotidal estuary sediments of Qua Iboe River, Gulf of Guinea, Organic Geochemistry, 170, 104461, https://doi.org/10.1016/j.orggeochem.2022.104461, 2022.

Valentine, D. L.: Adaptations to energy stress dictate the ecology and evolution of the Archaea, Nat Rev Microbiol, 5, 316–323, https://doi.org/10.1038/nrmicro1619, 2007.

Villanueva, L., Schouten, S., and Sinninghe Damsté, J. S.: Depth-related distribution of a key gene of the tetraether lipid biosynthetic pathway in marine T haumarchaeota, Environmental Microbiology, 17, 3527–3539, https://doi.org/10.1111/1462-2920.12508, 2015.

Wade, J. A., and B.C. MacLean. “The Geology of the Southeastern Margin of Canada, Chapter 5.” In *M.J. Keen and G.L. Williams (Eds), Geology of the Continental Margin of Eastern Canada*, 190–238. Geological Survey of Canada, The Geology of Canada, 1990.

https://doi.org/10.5194/egusphere-2025-1228
Preprint. Discussion started: 28 March 2025

Weijers, J. W. H., Lim, K. L. H., Aquilina, A., Sinninghe Damsté, J. S., and Pancost, R. D.: Biogeochemical controls on glycerol dialkyl glycerol tetraether lipid distributions in sediments characterized by diffusive methane flux, Geochem. Geophys. Geosyst., 12, Q10010, https://doi.org/10.1029/2011GC003724, 2011.

White, D. C., Davis, W. M., Nickels, J. S., King, J. D., and Bobbie, R. J.: Determination of the sedimentary microbial biomass by extractible lipid phosphate, Oecologia, 40, 51–62, https://doi.org/10.1007/BF00388810, 1979.

Wörmer, L., Lipp, J. S., Schröder, J. M., and Hinrichs, K.-U.: Application of two new LC–ESI–MS methods for improved detection of intact polar lipids (IPLs) in environmental samples, Organic Geochemistry, 59, 10–21, https://doi.org/10.1016/j.orggeochem.2013.03.004, 2013.

Wörmer, L., Lipp, J. S., and Hinrichs, K.-U.: Comprehensive Analysis of Microbial Lipids in Environmental Samples Through HPLC-MS Protocols, in: Hydrocarbon and Lipid Microbiology Protocols, edited by: McGenity, T. J., Timmis, K. N., and Nogales, B., Springer Berlin Heidelberg, Berlin, Heidelberg, 289–317, https://doi.org/10.1007/8623_2015_183, 2015.

Yoshinaga, M. Y., Kellermann, M. Y., Rossel, P. E., Schubotz, F., Lipp, J. S., and Hinrichs, K.: Systematic fragmentation patterns of archaeal intact polar lipids by high-performance liquid chromatography/electrospray ionization ion-trap mass spectrometry, Rapid Comm Mass Spectrometry, 25, 3563–3574, https://doi.org/10.1002/rcm.5251, 2011.

Zhang, Y. G., Zhang, C. L., Liu, X.-L., Li, L., Hinrichs, K.-U., and Noakes, J. E.: Methane Index: A tetraether archaeal lipid biomarker indicator for detecting the instability of marine gas hydrates, Earth and Planetary Science Letters, 307, 525–534, https://doi.org/10.1016/j.epsl.2011.05.031, 2011.

Zhang, Y. G., Pagani, M., and Wang, Z.: Ring Index: A new strategy to evaluate the integrity of TEX_{86} paleothermometry, Paleoceanography, 31, 220–232, https://doi.org/10.1002/2015PA002848, 2016.

Zorz, J., Li, C., Chakraborty, A., Gittins, D. A., Surcon, T., Morrison, N., Bennett, R., MacDonald, A., and Hubert, C. R. J.: *SituSeq* : an offline protocol for rapid and remote Nanopore 16S rRNA amplicon sequence analysis, ISME Communications, 3, 33, https://doi.org/10.1038/s43705-023-00239-3, 2023.